A&A 506, 845–856 (2009)
DOI: 10.1051/0004-6361/200912540

Astronomy & Astrophysics

The puzzling binary HD 143418⋆

J. Zverko[1], J. Žižňovský[1], Z. Mikulášek[2,3], J. Krtička[2], I. Kh. Iliev[4], I. K. Stateva[4], I. I. Romanyuk[5], and D. O. Kudryavtsev[5]

[1] Astronomical Institute, Slovak Academy of Sciences, Tatranská Lomnica, Slovak Republic
e-mail: zve@ta3.sk
[2] Department of Theoretical Physics and Astrophysics, Masaryk University, Brno, Czech Republic
[3] Observatory and Planetarium of J. Palisa, VŠB – Technical University, Ostrava, Czech Republic
[4] Institute of Astronomy, NAO Rozhen, Sofia, Bulgaria
[5] Special Astrophysical Observatory, Nizhnii Arkhyz, Russia

Received 20 May 2009 / Accepted 18 July 2009

ABSTRACT

Context. HD 143418 was discovered recently to be a double-lined spectroscopic binary with a primary designated as a CP star. Its light displays an orbital phase coupled variability with a peak-to-peak amplitude up to 0.04 mag.
Aims. The photometry available and new high dispersion spectra were investigated from a point of view of CP characteristics.
Methods. A series of high resolution high *S/N* coudé spectra was acquired from which 25 weak to strong unblended lines of Fe I and II, Ti II, Cr II, Zr II, and Ba II were selected to study spectral line variability. Two Zeeman spectra were obtained to search for a possible magnetic field of the star, and one echelle spectrum in a wide spectral region was analysed for abundance determination by means of synthetic spectra. The photometric observations were subjected to a PCA disentangling of the complex photometric behaviour.
Results. We identified spectral lines of the secondary in the yellow region on the echelle as well as on two coudé spectra, whose occurence belongs to an F6V star and the intensity corresponds to the luminosity ratio 0.06. Equivalent widths of the selected spectral lines of the primary component do not change within the errors of measurements. The spectra taken with a Zeeman analyser do not indicate a magnetic field. The abundance pattern does not correspond to characteristics of a variable CP2 star. The only remarkable deviation is a more than 1.1 dex deficit of scandium, one of the properties of non-variable Am stars. The photometric variability is tied to the orbital period and is due to ellipticity of the primary component and not to a putatively structured surface of the primary that is confirmed to rotate subsynchronously. The seasonal component of the light curve changes in amplitude as well as in shape.
Conclusions. We conclude that the primary is a normal, mildly evolved A5V main sequence star. The seasonal variability of the orbitally modulated light curves may be related to an expected incidence of circumstellar matter originating in the tidally spinning up primary component. HD 143418 may be a prototype of a rare detached interacting close binary containing a subsynchronously rotating primary passing through its synchronisation stage.

Key words. binaries: spectroscopic – stars: variables: general – stars: chemically peculiar – stars: abundances – stars: evolution – stars: individual HD 143418

1. Introduction

Chemically peculiar (CP) stars represent a significant class of stars occupying the upper main sequence where processes of radiative diffusion and gravitational settling in their atmospheres build up chemical abundances remarkably different from the solar ones. According to these chemical anomalies, they have been classified by Preston (1974) in to four subclasses from CP1 to CP4 that simultaneously follow a temperature sequence. Of these, CP1 (also named Am-stars) and CP3 (or MnHg-stars) almost exclusively occur in binaries, while the others are mostly single. On the other hand CP2 (or Ap-stars) and CP4 (He-weak, He-strong) stars possess strong global magnetic fields, and also demonstrate variability both of spectrum and light on timescales of the order of a day longer.

HD 143418 (HIP 78226) has long been used as a check star for photometric observations of the Be-star 4 Her (V839 Her). Božić et al. (2007) found HD 143418 to be variable while reducing their observations obtained in 2001, discovering its binary nature, and in a detailed analysis derived orbital parameters and physical characteristics of the components. They noticed a similarity of the light variability to light curves of some CP stars that can be described by a basic frequency and its first harmonic, and designated the primary as a CP star. However, they concluded that the *observed light variations can be understood as a combination of the ellipsoidal variability in the binary system and either a secularly varying pattern of spots on the secondary or an inhomogeneous corotating cloud ejected from the primary.*

Besides the photometric signs, a CP star manifests itself through horizontally uneven over/underabundances of some chemical elements, the spectral lines of which may vary in profile and/or strength. It is believed that the inhomogeneous surface distribution is a result of radiatively driven diffusion in a global magnetic field. Hot magnetic CP stars may also create and maintain corotating clouds.

A further important characteristic of CP stars is their occurrence in binaries. Budaj (1999), North et al. (1998), Mathys et al. (1997) and North (1994), and others have revealed that

⋆ Tables 5 and 6, and Fig. 14 are only available in the electronic form at http://www.aanda.org

Table 1. List of observations.

HJD 2450000+	Date dd/mm/yyyy	Phase	RV [km s^{-1}]	Region [Å]	S/N[1]	Obs/Instr[2]	Season
3536.38568	14/06/2005	0.273	–107.5	4855–4958	114	NAO/Coude	1
3537.37124	15/06/2005	0.701	50.4	4931–5033	162	NAO/Coude	1
3574.35386	22/07/2005	0.907	33.9	4459–4561	99	NAO/Coude	1
3575.35675	23/07/2005	0.346	–80.4	4457–4559	145	NAO/Coude	1
3600.27824	17/08/2005	0.265	–98.84	4461–4563	52	NAO/Coude	1
3601.31039	18/08/2005	0.717	53.3	4461–4563	92	NAO/Coude	1
3664.20447	20/10/2005	0.272	–107.3	4469–4561	107	NAO/Coude	1
3751.60595	16/01/2006	0.563	–2.6	4458–4560	116	NAO/Coude	2
3786.54807	20/02/2006	0.872	33.5	4461–4563	129	NAO/Coude	2
3787.54981	21/02/2006	0.311	–104.8	4461–4563	101	NAO/Coude	2
3963.30969	15/08/2006	0.313	–104.8	4464–4566	120	NAO/Coude	2
3965.30781	17/08/2006	0.189	–105.8	4465–4567	108	NAO/Coude	2
4187.51834	27/03/2007	0.542	–17.5	4461–4563	65	NAO/Coude	3
4286.38516	04/07/2007	0.857	36.7	4460–4562	105	NAO/Coude	3
4287.44814	05/07/2007	0.322	–113.2	4459–4562	50	NAO/Coude	3
4288.37642	06/07/2007	0.729	35.5	4459–4562	101	NAO/Coude	3
4289.30469	07/07/2007	0.136	–92.2	4459–4562	102	NAO/Coude	3
4290.31728	08/07/2007	0.579	–0.8	4459–4562	81	NAO/Coude	3
4336.28220	23/08/2007	0.717	34.3	4461–4564	110	NAO/Coude	3
4338.27705	25/08/2007	0.591	23.5	4461–4564	109	NAO/Coude	3
4541.59472	16/03/2008	0.662	37.1	4464–4567	84	NAO/Coude	4
4612.44306	25/05/2008	0.707	47.6	4458–4561	85	NAO/Coude	4
4641.35661	23/06/2008	0.370	–77.4	4463–4566	102	NAO/Coude	4
4642.36146	24/06/2008	0.810	53.8	4463–4566	111	NAO/Coude	4
4644.38047	26/06/2008	0.696	54.9	4462–4465	87	NAO/Coude	4
4925.51901	03/04/2009	0.869	30.8	5838–5941	154	NAO/Coude	5
4926.48301	04/04/2009	0.291	–104.7	5838–5941	188	NAO/Coude	5
4926.52917	05/04/2009	0.312	–96.2	6510–6612	158	NAO/Coude	5
4959.32832	07/05/2009	0.681	53.1	6468–6663	156	NAO/Coude	5
3514.27153	23/05/2005	0.584	18.9	4731–6137	210	SAO/Echelle	1
3520.47292	29/05/2005	0.301	–96.7	4389–4630	330	SAO/Zeeman	1
4955.39500	03/05/2009	0.941	13.0	4765–5005	440	SAO/Zeeman	5

[1] S/N is given for pixel in continuum; [2] "NAO/Coude" = coudé spectrograph of 2-m telescope at Rozhen Observatory, "SAO/Echelle" = NES at 6-m BTA telescope of SAO, "SAO/Zeeman" = Zeeman analyser of 6-m BTA telescope of SAO.

only a few systems with an Ap star component have an orbital period less of than 3 days, which is the case of HD 143418 with $P_{\rm orb} = 2.28252$ d.

Having the preliminary knowledge of Božić et al. (2007), we began a campaign of spectroscopic observations of the star in order to answer the question of whether HD 143418 is a true CP star or is not.

During the period 2005–2009 we obtained a collection of 32 high resolution, high S/N CCD spectrograms, among them 23 phase-resolved coudé spectra taken in the blue region, six coudé spectra in additonal regions, two spectra taken with a Zeeman analyser, and one broad region echelle spectrum.

In this paper we study HD 143418 to investigate its possible CP characteristics from the point of view of: i) light variability; ii) spectrum variability; iii) magnetic field; and iv) binarity.

2. Observations

The observations are listed in Table 1. The twenty-nine spectra from the National Astronomical Observatory, Rozhen, Bulgaria (NAO), were recorded using the photometric AT200 CCD camera with a SITe SI003AB 1024 × 1024 detector placed at the 3rd optical camera of the coudé spectrograph of the 2-m RCC telescope, with $R = 22\,000$. The $FWHM$ of the instrumental profile including the spectrograph optics corresponds to two pixels of size 0.2 Å. IRAF[1] standard procedures were used for bias subtracting, flatfielding and wavelength calibration. The echelle spectrum from the 6-m BTA telescope of the Special Astrophysical Observatory, Nizhnij Arkhyz, Russia (SAO), was taken with a 2048×2048 "Uppsala" CCD camera (Panchuk et al. 2002) of the Nasmyth Echelle Spectrometer (NES) with resolution $R = 50\,000$. The Zeeman spectra were obtained at SAO with the Zeeman analyser of the Main Stellar Spectrograph (MSS) at the 6-m BTA and CCD2 2048 × 2048 camera (Panchuk 1998), with $R = 16\,000$. The spectrograph optics in these two spectrographs blurs the instrumental profile over two detector pixels and corresponds to 0.237 Å in the Zeeman analyser of MSS, and 0.11 Å in the NES. The software package developed in the ESO MIDAS system (Kudryavtsev 2000) was used to reduce the SAO spectra.

3. Variability and magnetic field

Photometric and spectral variability of CP stars is a sign of a structured surface with spots of enhanced chemical abundances that, as is now accepted, originate in the processes of radiatively

[1] IRAF is distributed by the National Optical Astronomy Observatories, which are operated by the Association of Universities for Research in Astronomy, Inc., under cooperative agreement with the NationalScience Foundation.

driven diffusion in the global magnetic field of a star. As the star rotates, the spots moving across the visible hemisphere produce variations in light and spectral lines.

The long-term stability of observed light and spectral variations of CP stars indicates that the spectral and photometric spots are persistent on a time scale of many decades. Further, Mikulášek et al. (2007a) showed that the amplitudes of light curves of all CP stars are wavelength-dependent, so that there is no CP star with the same amplitude in all passbands.

3.1. Photometry and radial velocity

Notwithstanding that Božić et al. (2007) analysed the photometric behaviour of the HD 143418 binary thoroughly, we examine it again with the aim to confirm or disprove the classification of the primary component as a CP star.

All photometric observational data used in this section were taken from Božić et al. (2007), namely the 127 H_p measurements, 133 *UBV* observations done by APT-10, Phoenix, Arizona, USA, and 889 *UBV* observation done in Hvar (Croatia) and Ondřejov (Czech Republic) observatories. The observations from the SPM Observatory, Mexico, and from the Tubitak Observatory, Turkey, were not used because of their high level of noise and poor phase coverage. Thus the photometry of HD 143418 used in this paper covers the time interval 1982–2005, and represents in total 1149 measurements in four photometric passbands of different effective wavelength.

A brief inspection of the HD 143418 photometric data shows that the observed light variations are only moderate – a few hundredths of a magnitude modulated with the binary orbital period of 2.2825 days. The light curves observed in individual seasons are relatively smooth, so they are reminiscent of those of CP stars (Božić et al. 2007). Nevertheless, it seems that this similarity may be unreal – as evidenced in the detailed discussion in Sect. 5.2.1. The crucial reason why the observed light variations cannot be ascribed to the supposed chemical peculiarity of the primary component is the fact that it rotates subsynchronously (see Božić et al. 2007 and Sect. 4.2). Nevertheless, there still remains a possibility that after removing the orbital component from the variability, some variations typical for a rotating variable CP star could be found.

3.1.1. The orbital period

Božić et al. (2007) analysed the light and radial velocity variations of HD 143418 and found the orbital ephemeris for a superior conjunction of the primary:

$$T_{\text{sup. conj.}} = 2449178.43247(99) + 2.282520(10) \times E. \quad (1)$$

We developed a special robust regression code (for details see Mikulášek et al. 2008) that eliminates the influence of outliers on the period determination and enables treatment of various sets of photometric and radial velocity data simultaneously. Here the latter consists of the 12 original values taken from Božić et al. (2007) and the 32 ones added by us (see Table 1).

Radial velocities from the newly acquired spectra were derived using the CCF method described in Zverko et al. (2007). The template spectrum for the region 4460–4560 Å was prepared by coadding the corresponding 23 NAO spectra. As discussed in Sect. 4.1, the few strongest lines of the secondary component are not or at most questionably visible in this region; the resulting coadded spectrum represents practically a clean spectrum of the primary (see Figs. 9 and 10). For the remaining nine spectra the synthetic spectrum with abundances derived in Sect. 4.2 served as the template. The results are given in Table 1 and the radial velocity curve for the primary is displayed in Fig. 1.

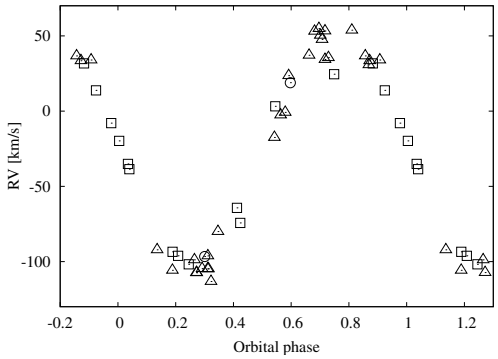

Fig. 1. Radial velocity folded with orbital phase according to Božić et al. (2007). Triangles - Rozhen spectra, circles – SAO spectra, squares – Božić et al. (2007).

The photometric data were divided into five consecutive eras of uneven duration with a comparable amount of observational data.

When constructing the simplest possible model of a light curve, we proposed that the real light curve contains a steady double-waved symmetric light curve corresponding to the proximity effects between the binary components, and a transient light curve caused by an unknown mechanism. Empirically, we found that the transient light curves could be represented by a harmonic function up to the first harmonic whereas the term with $\sin(4\pi f)$ (f is the orbital phase) can be neglected,

$$\begin{aligned} m_{ce}(t) \quad &\cong \quad \overline{m}_{ce} + A_{\mathrm{C}} \tfrac{4}{\sqrt{17}} \left[\cos(4\pi f) + \tfrac{1}{4}\cos(2\pi f)\right] \\ &+ \; a_{1e}\sin(2\pi f) + a_{2e}\tfrac{4}{\sqrt{17}}\left[\cos(2\pi f) - \tfrac{1}{4}\cos(4\pi f)\right], \quad (2) \end{aligned}$$

where $m_{ce}(t)$ is the magnitude of the model function, $\overline{m}_{ce}$ is the mean value of the magnitude, A_{C} is the effective semi-amplitude (see e.g. Mikulášek et al. 2007b) of the steady light variations due to the ellipticity of the primary component, a_{1e} and a_{2e} are partial effective semi-amplitudes describing the shape of the transient component of the light curve. The linear orbital phase is $f = (t - M_0)/P$, where time of observation t is counted in $\mathrm{JD_{hel}}$, M_0 is the time of the basic light minimum and P the period in days, c and e in subscript indicate passband and era respectively.

The model for the radial velocity phase curve assumes circular orbits of components so that

$$RV(f) \cong B\sin(2\pi f) + \gamma, \quad (3)$$

where B is the semi-amplitude of radial velocity of the primary component, γ is the mean radial velocity of the system.

Applying the regression code to the observational data and assuming the above specified models we get the main parameters of the variability, $B = -79.0 \pm 1.4\ \mathrm{km\,s^{-1}}$, $\gamma = -23.4 \pm 1.1\ \mathrm{km\,s^{-1}}$, and $A_{\mathrm{C}} = 0.00860(45)$ mag. In the result we obtain the shifts of the observed curves relative to the calculated ones in the individual eras, as displayed in Fig. 2. We arrived at the following linear ephemeris of photometric and radial velocity variations:

$$T_{\mathrm{minI}} = 2451454.136(7) + 2.282520(8) \times E. \quad (4)$$

The derived period is the same as the one in Eq. (1), its slightly higher accuracy results from the extension of the observational period through 2009.

As the distribution of the O–C points in Fig. 2 does not exclude a parabolic fit, we also tested the applicability of a

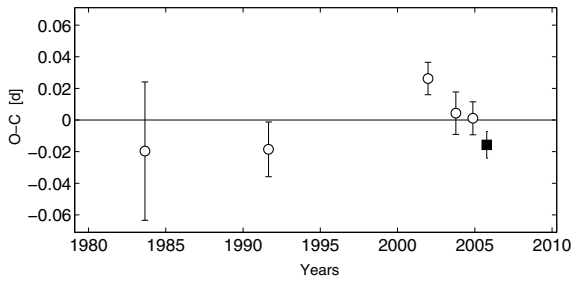

Fig. 2. O–C of orbitally modulated variations of HD 143418. Open dots – photometry, full squares – radial velocity data.

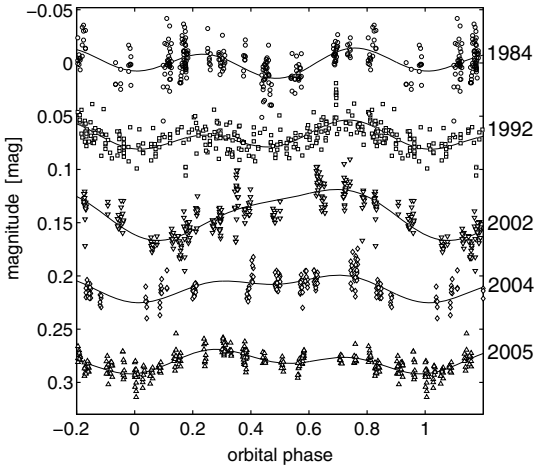

Fig. 3. The shapes of light curves in particular eras. The light curves are assembled from individual colour curves after subtracting their mean magnitudes within each era.

quadratic ephemeris in the form according to Mikulášek et al. (2008):

$$T_{\mathrm{minI}} = M_0 + P_0 \times E + \frac{1}{2} P_0 \dot{P} \left(E^2 - \frac{\overline{E^3}}{\overline{E^2}} E - \overline{E^2} \right), \quad (5)$$

where $\dot{P}$ is a derivative of the period, P_0 is the period in $t = M_0$. We found $\dot{P} = -8(6) \times 10^{-9}$, $\dot{P}/P = -1.2(1.0) \times 10^{-6}$ y^{-1}. Here the errors are comparable to the derived values itself, so the assumption of the quadratic term is rather questionable. Consequently, the linear ephemeris as quoted in Eq. (4) is a good approximation for the subsequent analyses.

3.1.2. PCA disentangling of light curves

In the following we analyse the development of the light curves of HD 143418 using the ephemeris Eq. (4). The light curves shown in Fig. 3 obtained in the five eras were subjected to the advanced principle component analysis (hereafter APCA) described in Mikulášek (2007).

APCA confirmed the anomalous and complex character of the long-term development of the light variations of HD 143418. In the result, we extracted a steady symmetric double-wave component with two equal maxima and unequally deep minima (see Fig. 5), and a seasonally changing component (see Fig. 4 and Table 2). The former was also noticed by Božić et al. (2007) and interpreted as the proximity effect common in the close binaries. The primary minimum of this component takes place at the orbital phase –0.002.

For quantification of the development of the complicated periodic light changes we used the effective semi-amplitudes as

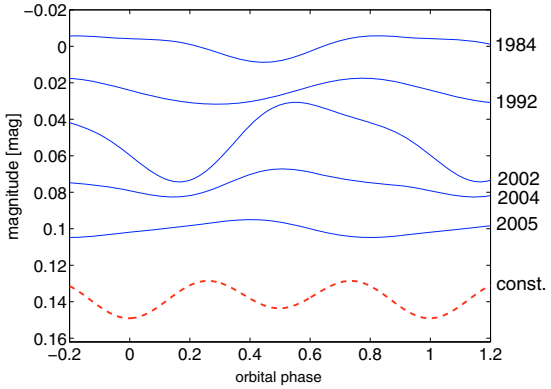

Fig. 4. Transient component of light curves in particular eras. The stable component is shown in the *bottom* for comparison of the amplitudes.

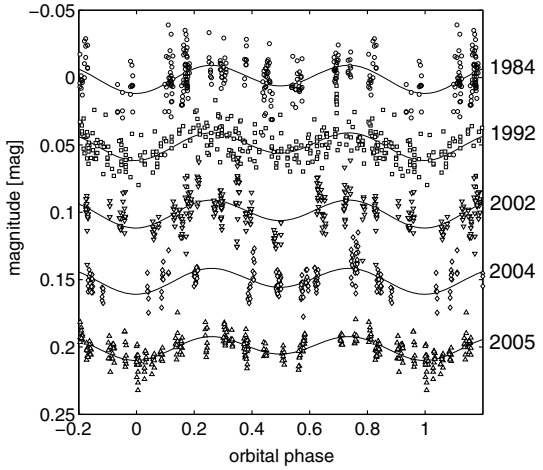

Fig. 5. Light curves after removing the transient component in particular eras.

defined e.g. in Mikulášek et al. (2007b), the seasonal A_{Se} and "steady" A_{Ce} components of the light curves, and the average magnitudes in *UBVHp* $\overline{m}_{ce}$ in individual eras e (see Table 2). It seems that the semiamplitude of the steady component remains constant, while the semiamplitude of the seasonal component varies considerably. We found a weak positive correlation between this quantity and the instant average magnitude $\overline{m}_{ce}$, which can be approximated in the form

$$\overline{m}_{ce} \cong \overline{m}_{c0} + \alpha\, A_{Se}, \quad (6)$$

where $\alpha = 0.31 \pm 0.22$, and $\overline{m}_{c0}$ is the mean magnitude in the passband c if the seasonal variability ceases. Apart from the large uncertainity of α, its positive sign means that the mechanism responsible for the observed seasonal phase variations causes the extinction of the star on average. The value of $\alpha < 1$ indicates that in some phases the system is brighter when unaffected by that mechanism. This is a supplementary constraint of possible mechanisms producing the observed light variations. The $\overline{m}_{c0}$ values are given in the last line of Table 2.

We also searched for a periodicity in the residuals, obtained after subtracting the modeled orbitaly modulated brightness, which could be attributed to variations of a subsychronously rotating CP2 star. We were unable to find any periodic variations with an amplitude exceeding 0.01 mag which is typical for weakly variable CP2 stars, see periodogram in Fig. 6. The highest peak is near the frequency 0.25 d^{-1} with a semi-amplitude of only 3.5 mmag, while no peak is indicated around the

Table 2. Disentangled characteristics of the light curves.

Era	Interval	N	A_{Se}	A_{Ce}	$\overline{m}_{Ue}$	$\overline{m}_{Be}$	$\overline{m}_{Ve}$	$\overline{m}_{Hpe}$
I	1982–87	273	0.0067(12)	0.0096(13)	7.7188(16)	7.6019(16)	7.4428(12)	
II	1989–99	260	0.0067(9)	0.0091(9)	7.7144(14)	7.6140(14)	7.4433(16)	7.4811(10)
III	2001–02	241	0.0205(11)	0.0094(12)	7.7150(17)	7.6128(17)	7.4492(11)	
IV	2003–04	174	0.0071(12)	0.0085(13)	7.7178(11)	7.6140(11)	7.4499(11)	
V	2004–05	237	0.0047(7)	0.0080(6)	7.7134(8)	7.6018(8)	7.4459(7)	
$\overline{m}_{c0}$			0	–	7.7126(26)	7.6050(25)	7.4440(26)	7.4791(42)

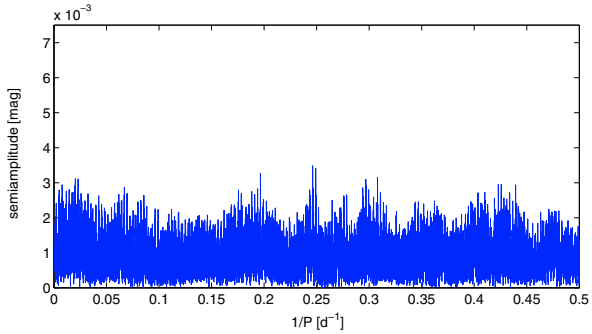

Fig. 6. Periodogram of magnitude residuals. Explanation in the text.

frequencies 0.07 d^{-1} corresponding to the 14 day subsynchronous rotational period of the primary. Consequently we conclude that the primary component of HD 143418 obviously does not belong to the group of photometrically variable CP2 stars.

3.2. Spectrum variability

The spectrum variability of a CP star consists either of variable line profiles with a moving narrow absorption feature from the blue to red wing of the line and/or variable equivalent widths. To investigate the former, line profiles must be sufficiently broadened due to rotation which is not the case of the primary component of HD 143418 with $v \sin i = 18$ km s^{-1} as derived by Božić et al. (2007). To investigate phase-to-phase variability of spectral lines we measured equivalent widths of 7 lines of Fe I (λ4466.55, iron blends at 4476.0 and 4482.2, 4484.22, 4494.56, iron blend at 4528.7, and 4547.8 Å), 8 lines of Fe II (λ 4472.93, 4491.40, 4508.29, 4515.34, 4520.22, 4522.63, 4541.52, and 4555.89 Å), 5 lines of Ti II (λ 4468.51, 4488.33, 4501.27, 4544.03, and 4545.13 Å), 3 lines of Cr II (λ4539.60, 4554.99, and 4558.65 Å), one line of Zr II at 4496.98 Å (which however, is blended with the Cr II line at 4496.842 Å) and one line of Ba II at 4554.03 Å. The code EQWREC2 of Budaj & Komžík (2000) was utilised for the measurements. Since all the lines of a species must originate in the same place, the equivalent widths of individual lines of an ion were summed and the sums were subjected to a period search using the Period04 code (Lenz & Breger 2005). The results of the period search down to the Nyquist frequency and the statistics are summarized in Table 3. The number of lines within a $\pm 2\sigma$ is given in the fifth column. The periods for the individual species are scattered randomly from 2 to 55 days and their amplitudes equal the limits at 1σ of the species' average. Thus the scatter of the equivalent widths is consistent with the measurement accuracy influenced mainly by the uncertainity in setting a local continuum.

Table 3. Results of the period search for the measured lines.

Ion	N	Mean	Extrema	$\pm 2\sigma$	P [d]	Ampl.	σ
Fe I	7	0.502	0.466–0.557	23	13.6	0.0274	0.027
Fe II	8	1.029	0.982–1.057	23	9.9	0.0229	0.024
Ti II	5	0.506	0.477–0.547	23	55.1	0.0189	0.019
Cr II	3	0.237	0.197–0.272	22	2.3	0.0189	0.018
Zr II	1	0.036	0.028–0.042	23	24.9	0.0066	0.007
Ba II	1	0.138	0.122–0.164	22	16.3	0.0091	0.009

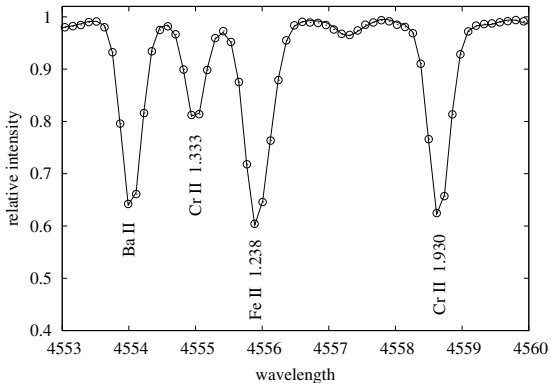

Fig. 7. Comparison of *right* (full line) and *left* (open circles) circularly polarised spectra. Numerical entry next the ion designation stands for the Lande factor.

3.3. Effective magnetic field

The CP stars exhibiting light and spectrum variability are known to have a global magnetic field that varies with the same period. As an example we use HD 119213, the cool CP star of SrCrEu type with an amplitude in Strömgreen's v, $A_v = 0.089$ mag (Mikulášek et al. 2007b), the period $P = 2.4499$ d and effective magnetic field $B_{\rm eff}$ varying from –0.5 to 1.2 kGs (Romanyuk 2004), the SrCrEu star HD 188041, $A_v = 0.090$ mag, $P = 223.81$ d (Mikulášek et al. 2007b), and a magnetic field varying from –0.2 to 1.5 kGs (Romanyuk 2004), the SiCr star HD 32633 with amplitude in u, $A_u = 0.048$ mag, $P = 6.4300$ d (Mikulášek et al. 2007b), and magnetic field varying from –5.7 to +3.5 kG. There is, however, the Si star HD 177410 with an amplitude in $A_u = 0.048$ mag and $P = 1.1233$ d (Krtička et al. 2009), with negative (or spurious so far, Kudryavtsev 2008, private communication) detections of a magnetic field. Measurements on two Zeeman spectra of HD 143418 resulting in $B_{\rm e} = -10 \pm 50$, and -70 ± 50 kGs, however, do not indicate an effective magnetic field exceeding the measurement errors. This finding is also documented in Fig. 7, where comparison of the right and left circularly polarised strips of one of the Zeeman spectra show thet they are identical.

The above analyses indicate that the primary component of the HD 143418 binary is not a CP2 star but allow that it

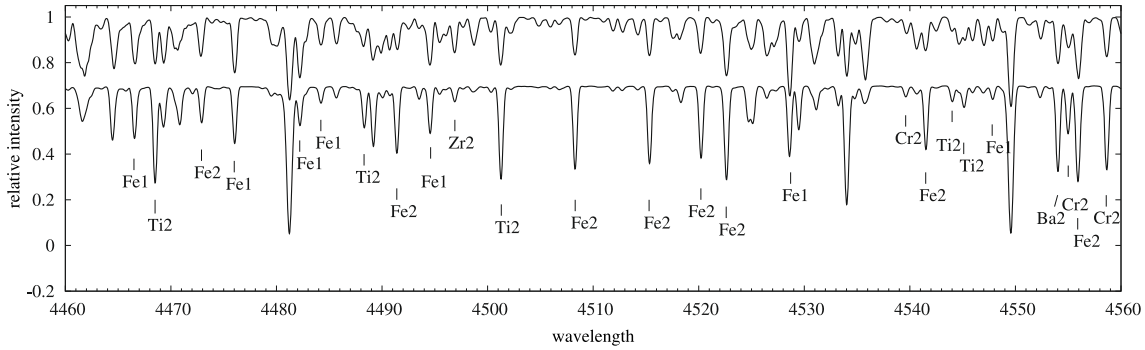

Fig. 8. Comparison of synthetic spectra of the primary and secondary computed for $T_{\rm eff}$(A) = 8190 K, $\log g$(A) = 3.85 and $T_{\rm eff}$(B) = 6550 K, $\log g$(A) = 4.4 respectively. The labeled lines were used in Sect. 3.2 to investigate the phase variability of equivalent widths. The primary spectrum is shifted down in intensity for clarity.

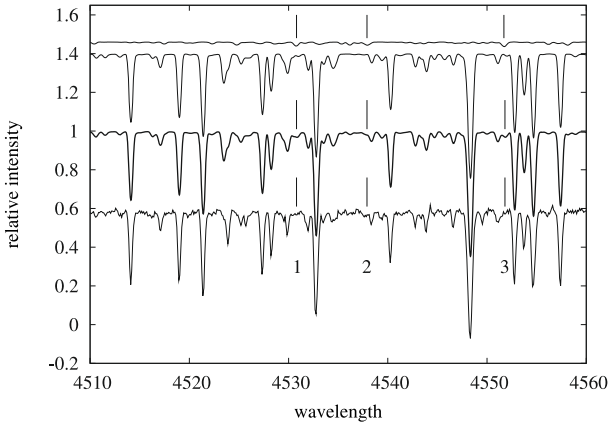

Fig. 9. Observed and composite synthetic spectra in phase 0.272. *From top to bottom* are shown secondary synthetic spectrum (×0.06), primary synthetic spectrum (×0.94), composite and observed. The vertical bars indicate lines in the secondary spectrum that should be visible in the observed but are not (label 1), possible (2) or disputable (3).

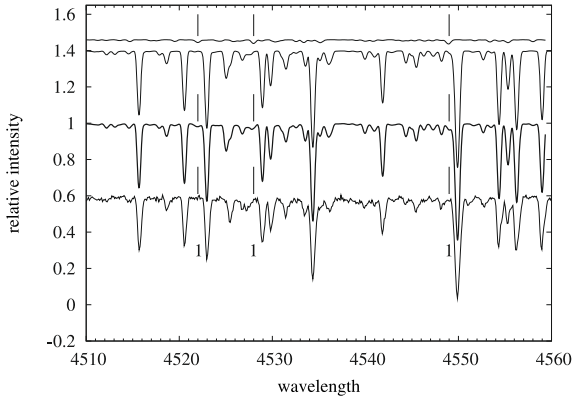

Fig. 10. The same as Fig. 9 but for phase 0.563.

might be a CP1 star. Nevertheless, only a thorough inspection of HD 143418 spectra and the chemical composition of the star could give a final decision.

4. Abundance analysis

The effective temperature and surface gravity of the primary component of HD 143418 place it among main sequence A stars. Provided that at the same time it is a CP star, we could expect that it belongs to the group of late CP2 stars of the SrCrEu subtype or Am stars. The SrCrEu CP2 stars feature strong lines of Sr II, Fe I, Fe II, Cr I, Cr II and rare earths, while the Am stars are characterised by enhanced lines of metals and weak lines of Ca II and Sc II. A brief inspection of the spectra does not show any apparent classification as an SrCrEu or Am star. Nevertheless, Božić et al. (2007) argued that "*the CaII lines are highly underabundant, which is a typical property of Am stars but less so of Ap stars. The overabundancy of CrII lines displayed in Fig. 8 is a characteristic of Ap as well as Am stars*". This is a striking discrepancy with our findings.

4.1. Composite spectra

Božić et al. (2007) detected the secondary component moving around the centre of Hα so prior to abundance analysis we checked how significantly the observed composite line spectrum can be affected by the secondary component.

We calculated synthetic spectra using SYNSPEC, Hubeny et al. (1994) modified by Krtička (1998) with effective temperature, surface gravity and projected rotational velocity values as derived by Božić et al. (2007), i.e. $T_{\rm eff}$(A) = 8190 K, $\log g$(A) = 3.85, $v \sin i$(A) = 18 km s^{-1}, $T_{\rm eff}$(B) = 6550 K, $\log g$(B) = 4.4, $v \sin i$(B) = 22 km s^{-1}, and solar scaled abundances. We used the Vienna atomic line database (Kupka et al. 1999, Kupka et al. 2000; Piskunov et al. 1995; Ryabchikova et al. 1997, hereafter VALD). For atmosphere models the *grids of models and fluxes (Atlas9-ODFNEW)* provided by Castelli & Kurucz (2003) was used. The models were interpolated to the values of the effective temperature and surface gravity. In all these calculations the synthetic spectrum was convolved with the rotational and instrumental line width of the corresponding spectrograph, as introduced in Sect. 2. The synthetic spectra are shown in Fig. 8. Besides Mg II 4481 Å, lines of Fe I, Fe II and Ti II are most noticeable in the spectrum of the secondary.

The computed spectra of the primary and secondary were summed for each phase of the observation using the radial velocities corresponding to the radial velocity curve solution, and the luminosity ratio $L_2/L_{\rm tot} \simeq 0.06$ after Božić et al. (2007). In this level of contribution, the central depth 0.39 of the strongest absorption at 4549.5 Å in the spectrum of the secondary, which is a blend of Ti II and Fe II, will be less than 0.023 in the composite which, at a S/N ratio ≈100, should still be visible. Two of the cases are shown in Figs. 9 and 10. Inspecting these figures carefully one can spot traces of the strongest lines of the secondary spectrum in the composite theoretical spectrum. However, nothing similar and unambiguous can be found in the observed ones.

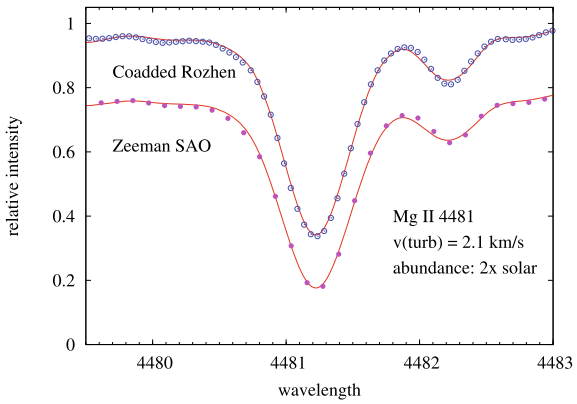

Fig. 11. Comparison of observed and synthetic profiles of the Mg II line at 4481 Å. The co-added Rozhen spectrum is fitted with $v \sin i$ = 18 km s^{-1}, the Zeeman SAO one with $v \sin i$ = 19 km s^{-1}.

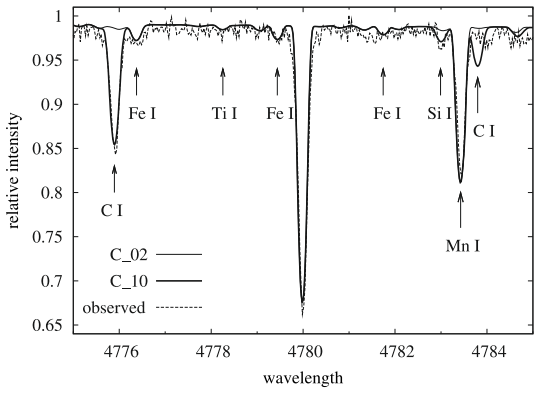

Fig. 12. Spectrum around 4780 Å. While the line of carbon at 4775.895 Å fits a normal abundance (thick line, labeled as C_10), the one at 4783.798 Å leads to an abundance multiplied by a factor of 0.02 (thin line, labeled as C_02). The strongest line belongs to Ti II. Here $v \sin i$ = 9.5 km s^{-1} as well as in Fig. 13.

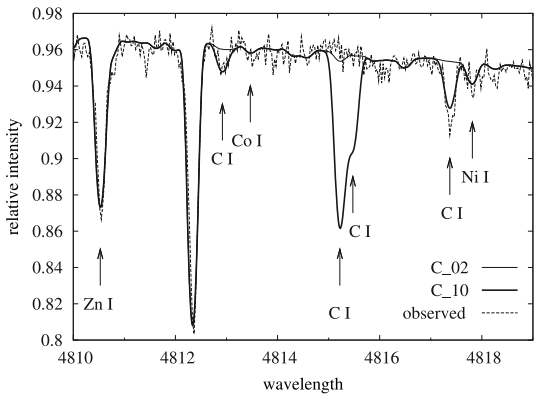

Fig. 13. Spectrum around 4815 Å. While the lines at 4812.920 and 4817.373 Å fit a normal abundance (thick line), the two at 4815.220 and 4815.475 Å fit an abundance multiplied by a factor of 0.02 (thin line). The strongest line belongs to Cr II.

The value of the luminosity ratio, however, was derived for the V band and thus it is obvious that in the blue region, the contribution of the cooler secondary is even smaller. Consequently, we consider the abundances derived from the Zeeman spectrum to be not contaminated by the lines of the secondary component.

In the echelle spectrum the luminosity ratio gradually increases with increasing wavelength. As shown in Fig. 14 we were able to identify the strongest lines of the secondary in the two coudé spectra and also in the echelle one in positions corresponding to the proper value of the radial velocity. The lines of the secondary could accidentally contaminate the lines belonging to the primary component, which if not resolved and if significant, could in the end lead to a positive wavelength dependency of the abundances derived, which however, was not found (see Sect. 4.2).

4.2. Deriving abundances

The abundance analysis was performed by calculating synthetic spectra as introduced in Sect. 4.1. In addition to the echelle spectrum, we used the first of the two Zeeman spectra in order to extend the spectral region down to shorter wavelengths.

First we estimated the value of microturbulence in the Zeeman spectrum by comparing the abundances derived from weak and strong lines of neutral and ionised iron. We needed $\xi_{\rm micro}$ = 3 km s^{-1}. For the Mg II 4481 Å line we used $\xi_{\rm micro}$ = 2.1 km s^{-1} and an abundance increased by a factor of 2 for the best result, see Fig. 11. This procedure was performed with $v \sin i$ = 19 km s^{-1} which also corresponds to the resolution of the Zeeman spectrum R = 16 000. When fitting the SAO echelle spectrum, however, a lower $v \sin i$ was found. This spectrum, with R = 50 000, allows a remarkably higher velocity resolution of 6.0 km s^{-1}. Here $v \sin i$ = 9.5 km s^{-1} is enough to fit the sharp line profiles, as can be seen in Figs. 12 and 13. The microturbulence derived for the echelle spectrum is ξ = 2.1 km s^{-1}. While abundances of the majority of elements were derived easily, resulting abundances of carbon, magnesium and silicon derived from particular lines are scattered within an order of magnitude. Therefore, besides VALD, semiempirical databases of Kurucz, R. L., & Peytremann, E. (1975, hereafter KP75) and Kurucz, R. L., & Bell, B. (1995, KB95), and Ralchenko et al. (2008, NIST) also were consulted. For other elements, a better agreement of a synthetic with observed line was sought for when desirable. The strength of the lines used in the analysis ranges from very weak with central intensities $I_{\rm c} \gtrapprox 0.95$, through weak, $I_{\rm c} \approx 0.9$, and medium $I_{\rm c} \approx 0.8$–0.7 to very strong with $I_{\rm c} \lessapprox 0.6$. In the following we introduce the results of the abundance determination and comment in detail on some discrepancies.

CARBON, oxygen and sodium lines were only identified on the echelle spectrum. We used 72 lines of C I that were not or only marginally blended with other elements. Thirty-seven fit normal abundance, some of them, however, fit better when a gf-value from another database is used (see Table 6). Thirty-three lines need the value of abundance multiplied by a factor of 0.02. These lines are not included in the NIST database, the KB95 is practically identical with VALD and the corresponding values at KP75 do not differ significantly. Two lines, at 5693.109 and 6013.165 Å, do not fit with the gf-values available. The latter is a blend of two carbon lines and the corresponding absorption feature would be reproduced sufficiently by a synthetic profile if one of them were taken with an abundance factor of 0.02 (See also Table 6). The abundance factor of 0.02 is the upper limit at which we arrived in successive steps until the lines vanish from the synthetic spectrum in accordance with the observed one. We illustrate the discrepancy between the two groups of C I lines in Figs. 12 and 13.

OXYGEN. Lines of O I are weak and/or very weak both in the synthetic and observed spectrum. For the 3 lines at 4772.446, 4773.775 and 4967.374 Å the abundance had to be decreased in successive steps to a factor of 0.2 in order to remove them from the synthetic spectrum. Two lines fit the abundance reduced by

factors of about 0.5, and 2 lines fit the normal one with gf-values from NIST.

SODIUM is normal for 3 weak to medium-strength lines of Na I.

MAGNESIUM. Despite magnesium being found in mild excess when fitting the strongest line of Mg II at 4481 Å, the remaining very weak to medium lines of Mg II and of Mg I identified on the Zeeman spectrum fit the solar abundance. This is the case also for the very weak to strong lines of Mg I identified in the echelle spectrum. However, the 4 lines of Mg II, weak in the synthetic spectrum, are still weaker in the observed one. These lines of Mg II need abundances multiplied by a factor of 0.3.

SILICON had to be multiplied by a factor of 0.03 to remove the lines of Si I and Si II present in the synthetic spectrum but absent in the observed Zeeman one. In the echelle spectrum, however, silicon is found in a dichotomy similar to carbon. Fourteen lines of Si I, four of them with gf-values from KB95, and three identified lines of Si II hint at a weak underabundance by a factor of 0.8. The gf-values for the four Si I lines are based on measurements of emission lines by Garz (1973) and revised by Lambert & Luck (1978) using the solar carbon abundance. Eighteen lines of Si I need to be multiplied by a factor of 0.03. Of these, 16 lines indicated in the synthetic spectrum as very weak are not present in the observed one, two at 4792.213 and 4792.324 Å are weak and one at 5006.059 Å is strong. However, different sources of gf-values admit different interpretations of observations. For example the Si I line at 5846.612 Å, which needs the abundance factor 0.03, has $\log gf = -1.832$ according to VALD, and –2.730 according to Kurucz & Bell (1995). The latter value, however, shifts the line into the other group that shows mild (a factor of 0.8) underabundance. Further, the line Si I at 6042.399 Å has $\log gf = -1.309$ and –4.300 according to VALD and Kurucz & Bell (1995) respectively. Using the VALD data leads to a relatively consistent group of lines giving an abundance multiplied by a factor of 0.03. Thus any selective choice of a "better" value from Kurucz & Bell (1995) in these cases would not be justified.

SULPHUR has to be multiplied at least by a factor of 0.3 to remove the lines of S I at 4429.142 and 4431.435 Å from the synthetic spectrum, which is only the upper limit for the abundance. For the lines identified on the echelle spectrum, the abundance must be multiplied by a factor of 0.05 in order to remove them from the synthetic spectrum.

CALCIUM is normal for all the lines of Ca I with KB95 values and the Ca II with the KP75 ones, identified on the Zeeman spectrum. On the echelle it is in a mild excess by a factor of 1.4. With this value, 6 strong, 7 medium and 3 very weak lines of Ca I fit excellently. Also 11 lines of Ca II, of which 2 are strong, 1 medium and 8 weak or very weak, fit excellently to the observed spectrum, three weak lines of them, however, with gf values from KP75.

SCANDIUM is found to be in deficit by factor of 0.075 for the 14 lines of Sc II identified in the Zeeman and echelle spectrum.

TITANIUM. Twenty lines of Ti I and 57 lines of Ti II, very weak to very strong, were identified in both spectra. Titanium is mildly overabundant by a factor of 2.

VANADIUM is normal or might be in weak deficit. Only a few weak or very weak lines are indicated in the synthetic spectrum and are visible as a trace in the observed echelle one. The KP75 gf-values, which are lower, fit better.

CHROMIUM is normal for 13 lines of Cr I and for 53 lines of Cr II identified in both spectra. The lines range from very weak to very strong.

MANGANESE was only identified on the echelle spectrum. Thirteen lines of Mn I and 4 lines of Mn II suggest a mildly increased abundance by a factor of 1.5. They are of very weak to medium strength.

IRON is normal. Thirty lines of Fe I and 16 lines of Fe II in the Zeeman spectrum, and 252 lines of Fe I and 78 lines of Fe II in the echelle spectrum were used. They range from very weak to very strong in strength. Two lines in the echelle spectrum do not fit with either gf-value.

COBALT. Only 2 very weak lines of Co I were identified in the echelle spectrum, they indicate normal abundance.

NICKEL is normal. Only 2 weak unblended lines were found in the Zeeman spectrum. The normal abundance also fits the absorption features in which nickel lines occur blended with Fe I and Ti II, such as those at 4459.027, 4462.449, 4470.472 and 4592.542 Å which, however, were not used for iron and titanium abundance determination and are not included in Table 5. Also 41 lines of Ni I used in the echelle spectrum satisfy normal abundance. In majority the lines are very weak or weak, five are medium-strong.

COPPER was identified only in the echelle spectrum and is underabundant. Five lines of Cu I were indicated as weak or very weak in the synthetic spectrum. In order to reach agreement with the observed spectrum we multiplied the abundance by a factor of 0.2. This way two of the lines, at 5220.066 and 5782.127 Å became invisible in the synthetic spectrum, in accordance with the observed one.

ZINC. One weak line of Zn I at 4810.528 Å was identified in the echelle spectrum and fits normal abundance.

YTTRIUM is mildly overabundant by a factor of 1.8 for 18 lines identified in the echelle spectrum. Four of them are medium strong, 2 are weak and the remaining 12 are very weak. The very weak line at 5781.689 Å while indicated in the synthetic spectrum with the VALD gf-values, is absent in the observed one consistent with the KP75 values.

ZIRCONIUM is in a mild excess by a factor of 1.5. Only 1 very weak line of Zr II was identified in the echelle spectrum. All of the 4 weak lines of Zr II identified in the Zeeman spectrum occur in blends with Ti I, Fe I,Fe II, Cr I and Mn I. The fits of the observed and synthetic spectrum in all these cases are very good, thus indirectly confirming the mildly increased abundance.

BARIUM is overabundant by a factor of 2.5 for the strong line of Ba II at 4554.029 Å and by a factor of 1.9 and 4 for the weak unblended line of Ba II at 5853.668 Å and the strongest line at 4934.076 Å respectively.

We tested the internal accuracy of the determination on 9 weak lines of titanium and differences in the computed profiles were fairly discernable when the abundance factor of 2 with a step 0.1 was varied. Taking the signal noise into account, the factor lies within 2 ± 0.2 for weak lines where $S/N \approx 100$ and 2 ± 0.3 for strong lines where $S/N \approx 70$ at their centres. Consequently, the accuracy of a derived abundance is ≈0.05–0.15 dex.

Thus, Na, V, Cr, Fe, Co, Ni and Zn are normal. Ca, Ti, Mn, Y, and Zr are mildly overabundant within the scatter resulting from the accuracy of determination and obvious for normal main sequence stars. Barium is mildly overabundant with a remarkable scatter in values resulting from three lines. O, S, Sc and Cu are underabundant. C, Mg and Si show discrepancies either within an ion or between neutral and singly ionised atoms. The results are summarised in Table 4, where the abundances are expressed in terms of a *factor* (deficit < 1 < excess). The "solar" values are from Asplund et al. (2005).

Table 4. Abundances of elements relative to solar values in the primary component.

Ion	A.factor Zeeman	*n*	A.factor echelle	*n*	Ion	A.factor Zeeman	*n*	A.factor echelle	*n*	Ion	A.factor Zeeman	*n*	A.factor echelle	n
C I			1.0	35	S I	<0.3	2	0.05	4	Fe I	1.0	30	1.0	255
			0.02	35	Ca I	1.0	9	1.4	16	Fe II	1.0	16	1.0	78
O			0.2	3	Ca II	1.0	2	1.4	11	Co I			1.0	2
			0.5	4	Sc II	0.75	4	0.075	8	Ni I	1.0	2	1.0	41
Na			1.0	4	Ti I	2.0	3	2.1	17	Cu I			0.2	5
Mg I	1.0	1	1.0	8	Ti II	2.0	29	2.1	28	Zn I			1.0	1
Mg II	1.0	4	0.3	4	V II			1.0	8	Y II			1.8	18
	2.0	1			Cr I	1.0	4	1.0	21	Zr II	1.5	4	1.5	1
Si I			0.8	14	Cr II	1.0	8	1.0	32	Ba II	2.5	1	1.9	1
	0.03	7	0.03	18	Mn I			1.5	13				4.0	1
Si II	0.03	2	0.8	3	Mn II			1.5	4					

We stress that the abundances were derived without including the ellipticity of the primary component of this binary as determined by Božić et al. (2007). The ellipticity may result in an additional limb darkening due to gravity, and the proximity of the components in a possible irradiation of the "sub-secondary" region of the primary. However, as seen from calcium, titanium, chromium, manganese or iron, where all lines fit one value of abundance the discrepancies present in other elements, e.g. carbon, are obviously not due to the mentioned effects.

Complete lists of the lines used in the abundance analysis are compiled in the on-line Table 5 for the Zeeman spectrum and Table 6 for the echelle one. VALD critically evaluates the accuracy of values introduced by variuos databases and recommends the best assessed one. If the best VALD value does not meet the observed strength of a line, a value from another database was used and is given in the fifth column and its source in the last column of the on-line tables. In the case when none of the abovementioned databases is considered by VALD, its value is given in the fifth column, while a more convenient other value and its source is given in the last one. In some cases, neither of the databases offers a *gf*-value able to fit the observed feature (this is marked with DNF = *does not fit* in the on-line tables). As many lines indicated in the synthetic spectrum are not visible in the observed one (marked as MIO = *missing in the observed* in the on-line tables), we investigated spectra of two other stars with similar temperature and gravity parameters to verify the absence of these lines as found in HD 143418. We used HD 27411 (A3m), and HD 148898 (A6p), published in the frame of *the UVES Paranal Observatory project* by Bagnulo et al. (2003). Though these stars are peculiar, we selected them due to their relatively slow rotation as the large $v \sin i$ of *normal* A stars would erase these very weak features. Similarly to HD 143418, the lines were found to be missing in these two stars, too. The discrepancies discussed in this section point to a strong need for improvement of the corresponding atomic data.

5. Discussion

5.1. Subsynchronous rotation of HD 143418 A

One of the important results of this work is the confirmation of the subsynchronous rotation of the primary component discovered by Božić et al. (2007). Accepting their geometric parameters of the binary, $P_{\rm orb} = 2.282520$ d, $i = 65.3°$, $R_\star = 2.67\ R_\odot$ and assuming that the rotational axis is perpendicular to the orbital plane, the projected rotational velocity $(v \sin i)_{\rm syn}$, according to the formula

$$(v \sin i)_{\rm syn} = \frac{50.613\, R}{P} \sin i, \qquad (7)$$

for synchronous rotation is $(v \sin i)_{\rm syn} = 54\ {\rm km\,s^{-1}}$. Nevertheless, we found the value $v \sin i \cong 9.5\ {\rm km\,s^{-1}}$ (see Sect. 4.2), and thus the rotation of the primary component is subsynchronous by a factor of 5 or more, corresponding to a rotational period of 14 days. To our knowledge, there is no other close binary with such a slowly rotating primary.

5.2. Is HD 143418 A a CP star?

The primary component of the unusual close binary HD 143418 was classified as an Am (CP1) star by Bartaya (1979) and recently again by Božić et al. (2007) who did not exclude that it even could be an Ap star (CP2 type) (see Sect. 4). These classifications were based on spectrum and partly on photometric diagnostics.

5.2.1. Is HD 143418 A a CP2 star?

If HD 143418 A with an effective temperature of about 8000 K is a CP2 star, it should be a cool Ap star of an SrCrEu subtype. Spectra of SrCrEu CP2 stars are dominated by plenty of strong lines of overabundant chemical elements, namely Sr II, Fe I, Fe II, Ti I, Ti II Cr I, Cr II and rare earths. The overabundant elements are distributed unevenly, forming various spots which result in the observed rotationally modulated spectral line variations (spectroscopic spots) as well as strong or moderate light changes from several hundreds to a few tenths of magnitude (see e.g. Mikulášek et al. 2007a) (photometric spots). The SrCrEu-type stars are known to have strong dipole-like magnetic fields of up to several kGs.

Providing the bound rotation of the photometrically dominant primary component, its light changes could be produced by the mentioned photometric spots on its surface. However, there are at least three arguments against this interpretation: (i) the amplitudes and forms of the orbitally modulated light variations conspicuously change from season to season, which is quite unusual for a single CP2 star. The only known CP2 star exhibiting moderate seasonal changes in its light curve is 56 Ari (Shore & Adelman 1976; Žižňovský et al. 2000; Adelman et al. 2001). These, however, are due to precession of the rotational axis of the magnetically distorted star; (ii) the amplitudes of the light variations in different colours in the same moment are almost equal, and (iii) the rotation of the HD 143418 A is subsynchronous. Consequently, the observed variations have to be produced by other mechanisms, as discussed in Sect. 5.2.3. Thus, the observed photometric variability studied in Sect. 3.1.2 is not the variability of a CP2 star.

We also searched for a periodicity in residuals obtained after subtracting the modelled orbitally modulated light variations which could be attributed to variations of a subsychronously

rotating CP2 star. We were not able to find any periodic light variations which are symptomatic of moderately variable late CP2 stars.

We measured equivalent widths of unblended or only marginally blended lines of iron, chromium and titanium, the species commonly found to create *spots*, and of zirconium and barium, the heavier elements found in a weak excess. As it is justified to suppose that all lines of a specific element or ion originate in the same (fiducial) spot, we summed the equivalent widths of the lines concerned. Only in two cases, chromium and barium, does one of the 23 values exceed the 2σ limit. The values were subjected to a period finding with negative results. As CP2 stars demonstrate the variability of equivalent widths of spectral lines with amplitudes often extending to double of their mean value (Wolff 1983; Polosukhina et al. 1999; Zverko et al. 1998), we conclude that the visible (primary) component does not show that spectrum variability proper to the CP2 stars.

A magnetic field of a simple dipolar or more complex structure, varying in intensity, is the third characteristics of CP2 stars demonstrating light and spectrum variability. It is believed the magnetic field governs the radiatively driven diffusion to create the structured surface of variable CP2 stars. Two observations with Zeeman analyser however, did not show evidence of a magnetic field of HD 143418 exceeding the measuring accuracy.

We state that the abundances of most of the studied elements are very near to solar ones. The cool CP2 stars showing light and spectrum variability have overabundances mainly of the rare earths often exceeding 3 dex, which is not observed in HD 143418. Moreover, no lines of any of the rare elements were identified in the whole spectral region studied in this work.

All the above summarized features, supported also by the fact that the CP2-type stars are very uncommon in short-period binaries such as the one studied in this paper, we conclude that the primary of HD 143418 is definitely not a CP2 star.

5.2.2. Is HD 143418 A an Am star?

With regard to the fact that the Am stars occur almost exclusively in binary systems, it is justified to examine the primary HD 143418 from the point of view of its Am-type peculiarity. The Am (CP1) stars are less conspicuous than the CP2 stars – they do not demonstrate photometric nor spectroscopic variability nor a magnetic field. The Am stars are characterised by overabundance of metals accompanied with underabundance of scandium and calcium. An Am star is horizontally chemically homogeneous. A further important characteristic is a relatively slow rotation (equatorial velocity below 100 $\mathrm{km\,s^{-1}}$), which is believed to be a necessary and may even be a sufficient condition for the origin and evolution of the Am phenomenon.

Accordingly the classification of this star as an A3m by Bartaya (1979), we found a strong deficit of scandium, which is one of the common characteristics of Am stars. On the other hand the derived abundance of calcium, the another element to appear in deficit, is found in a mild overabundance for 27 lines identified in the echelle spectrum.

The abundance pattern found in HD 143418 does not imply that the primary is an Am star.

5.2.3. Why is it not an Am star? A possible synchronisation scenario

The findings discussed above contradict our current understanding of the Am phenomenon. An evolved main sequence star with $T_{\rm eff} = 8190\,\mathrm{K}, \log g = 3.85$ and a very slow rotation with $P_{\rm rot} \approx 14$ day should be an Am star. However, we do not find any convincing evidence of the Am abundance anomalies except that of the deficit of scandium.

A key to comprehension of the oddness of HD 143418 may come from studies of Budaj (Budaj 1996, 1997, 1999) who demonstrated that tidal forces between components of a close binary would not affect the peculiar chemical composition of outer layers of the Am component only in the case that it rotates synchronously. If the Am component rotates non-synchronously, the tidal forces distorting the star from its spherical shape are able to destroy its anomalous stratification of chemical elements due to mixing of the surface layers on a short time scale. Note also that the reflection effect in non-synchronous binary components may affect radiative diffusion (Tassoul & Tassoul 1988).

Though the phenomenon of a subsynchronously rotating primary component in close binaries is not common, it deserves our interest, as does the process of synchronisation which has not been fully understood up to now (for more details see c.f. Claret et al. 1995; Khaliullin & Khaliullina 2007). Nevertheless, there are several systems with a plausible scenario for HD 143418. This is the case of the eclipsing binary V624 Her (HR 6611) with two evolved Am components, where the primary has a subsynchronous rotation, though the difference between its observed $v \sin i = 35\ \mathrm{km\,s^{-1}}$ and the synchronised $v \sin i = 39\ \mathrm{km\,s^{-1}}$ is not as distinctive as in the case of HD 143418 (Mikulášek et al. 2004). Popper (1984) claimed that *V624 Her appears to be more evolved in the mass-radius, temperature-gravity, and HR diagrams than any other Am star that has all properties well determined*. The subsynchronisation of it could be satisfactorily explained as the consequence of a relatively fast expansion at the end of its main sequence era. Projecting the values of temperature and radius of V624 Her on to the plane of Fig. 15 in Božić et al. (2007) we find it a little above HD 143418.

A larger difference between the synchronized and observed $v \sin i$ was found in the triple system DG Leo by Frémat et al. (2005). For its inner binary consisting of two Am stars of equal mass, with $P_{\rm orb} = 4.15$ d, the projected value of synchronous rotation is $v \sin i = 36\ \mathrm{km\,s^{-1}}$. One component, however, rotates faster, $v \sin i = 42\ \mathrm{km\,s^{-1}}$, while the other is subsynchronous with $v \sin i = 28\ \mathrm{km\,s^{-1}}$. The wide component, although of very similar mass and radius, rotates slowly too, but in contrast to the inner pair does not show any signs of peculiarity.

Griffin (2002, 2004, 2008) studied the 14.5-day binary o Leo consisting of an F8m and A7m components. While the cooler component rotates nearly synchronously with $v \sin i = 8.1\ \mathrm{km\,s^{-1}}$, the hotter one is remarkably subsynchronous with $v \sin i = 11.0\ \mathrm{km\,s^{-1}}$ corresponding to a rotation rate of 22 d. This component was found in its fast state of evolution and the slow rotation ascribed to its quick expansion.

However, any rebuilding of the star during the stay on the main sequence cannot lead to such a pronounced subsynchronisation of the primary as we find in HD 143418. Thus the rotation of the primary component was extremely slow during the whole preceding evolution. When the primary was near the ZAMS, its radius was considerably smaller than now and consequently the tides had been distorting the star only negligibly, as the efficiency of tides is $\propto R^3$. It is possible that some time ago the primary was an ordinary Am star. But it is possible that the radius of the star has grown to such a degree that the tidal interaction between the components is spinning up the primary more efficiently. A part of the orbital angular momentum is transformed into the rotational angular momentum of the primary, which leads to a decrease of the orbital period and brings the components closer, which

further amplifies the tides, and the process accelerates. This fast phase will terminate at the moment when the primary rotates synchronously. It is very likely that we observe HD 143418 during the onset of this fast evolution. The scenario could be tested by a very careful photometric and spectroscopic period monitoring in the future.

In the following we estimate the result of such a fast phase of evolution. Let J be the norm of the total angular momentum vector $\boldsymbol{J}$ of the system compound of almost spherically symmetric primary (1) and secondary (2) components with masses M_1, M_2, radii R_1, R_2, rotating with angular velocities Ω_1, Ω_2 circularly orbiting (assuming that orbital circularisation has passed) with angular orbital velocity Ω. We assume that the rotational axes of the both components are perpendicular to the orbital plane. Thus the sum of the orbital and rotational angular moments is

$$J = \mu a^2 + I_1\,\Omega_1 + I_2\,\Omega_2, \text{ whereas } a^3\,\Omega^2 = G\,(M_1 + M_2), \qquad (8)$$

where I_1 and I_2 are moments of inertia of the binary components, μ is the reduced mass of the binary, $\mu = M_1 M_2/(M_1 + M_2)$, and a is the separation of the components, G is the gravitational constant. It is very likely that the rotation of the secondary is always nearly bound, hence $\Omega_2 = \Omega$.

Let $a_0, \Omega_0, \Omega_{1,0}, P_0$ be instant values of the above introduced quantities. At the end of the synchronisation, both the angular velocities are equal to $\Omega_{\rm syn}$ and the separation of the components a_0 will change to $a_0 + \Delta a$. For simplicity we assumed that the process runs quickly, without apparent changes of the outer and inner characteristics of the components. Further, we consider that the process of synchronisation is conservative (any escape of matter from the system is neglected) and the total angular momentum J does not vary with time.

Applying a series expansion and justified neglected terms (the term with I_2 can be neglected because of $I_2 \ll \mu a^2$, etc.) we arrived at the following prediction of the synchronised state:

$$\Delta\Omega = \Omega_{\rm syn} - \Omega_0 \cong \frac{3\,I_1}{\mu a_0^2}\,(\Omega_0 - \Omega_{1,0})\,, \qquad (9)$$

where Ω_0 and $\Omega_{\rm syn}$ are the present angular velocity and the one after synchronisation respectively.

$$\frac{\Delta P}{P_0} \cong -\frac{\Delta\Omega}{\Omega_0}; \quad \frac{\Delta a}{a_0} \cong -\frac{2\Delta\Omega}{3\,\Omega_0}\,. \qquad (10)$$

The present state according to Božić et al. (2007) and this paper is characterised by $M_1 = 1.81\,M_\odot$, $M_2 = 1.09\,M_\odot$, $R_1 = 2.65\,R_\odot$, $R_2 = 1.1\,R_\odot$, $P_{1,0} \simeq 14$ d, $P_0 = 2.2825$ d, and the separation of the components $a_0 = 10.40\,R_\odot$. The momentum of inertia of both components can be approximated by $I_{\rm i} = \eta_{\rm i}\,M_{\rm i}\,R_{\rm i}^2$, where coefficients $\eta_{\rm i}$ quantify the mass distribution in stars; for a ZAMS star $\eta \simeq 0.1$ and as the star evolves, η monotonically decreases (Meynet & Maeder 2006). We estimated the values of $\eta_{\rm i}$ to be $\eta_1 = 0.05$ and $\eta_2 = 0.08$. During the synchronisation the orbital period will be reduced by 2.1% to $P_{\rm syn} = 2.23$, the components will move closer by 1.4% to $a_{\rm syn} = 10.26\,R_\odot$.

The total energy E of a gravitationally bound binary system with a synchronised rotation can be expressed:

$$E = -\frac{GM_1M_2}{2\,a} + \frac{I_1\,\Omega_1^2}{2} + \frac{I_2\,\Omega^2}{2}\,. \qquad (11)$$

A fraction of the orbital energy released during the synchronisation, $\Delta E_{\rm rot1}$ and $\Delta E_{\rm rot2}$ (the latter can be neglected), is consumed in spinning up the components, and the another, $E_{\rm diss}$, is dissipated mostly in the interior of the primary component.

$$\Delta E_{\rm rot1} \cong \tfrac{1}{2}\,I_1\,(\Omega_0^2 - \Omega_{1,0}^2); \quad E_{\rm diss} \cong \tfrac{1}{2}\,I_1\,(\Omega_0 - \Omega_{1,0})^2. \qquad (12)$$

We estimated the value of $\Delta E_{\rm rot1} \cong 3.0 \times 10^{38}$ J. The amount of the dissipated energy is smaller: $E_{\rm diss} \cong 2.2 \times 10^{38}$ J. We suspect that the dissipated energy might supply the activity of the primary.

By differentiating Eqs. (8) and (11) with respect to time we find the relation between the actual dissipative energy output $\dot{E}_{\rm diss0}$ and the expected shortening of the present orbital period $\dot{P}_0$

$$\dot{E}_{\rm diss0} \cong -\frac{GM_1M_2}{3\,a_0}\left(1 - \frac{\Omega_{1,0}}{\Omega_0}\right)\frac{\dot{P}_0}{P_0} = -2.0 \times 10^{40}\ {\rm J}\ \frac{\dot{P}_0}{P_0}\,. \qquad (13)$$

For $\dot{P}_0/P_0 = -1.2(1.0) \times 10^{-6}\ {\rm y}^{-1} = -4(3) \times 10^{-14}\ {\rm s}^{-1}$ found in Sect. 3.1.1 as a consequence of synchronisation we get for the dissipated energy output a hardly acceptable value $E_{\rm diss0} = 8 \times 10^{26}\ {\rm J\,s}^{-1} = 2.1(2.0)\,L_\odot$. The orbital acceleration is obviously lover by several orders and therefore not currently observable.

5.3. Spots on the secondary or ejected clouds?

Božić et al. (2007) offers two physical reasons that could plausibly explain the observed seasonal variation of HD 143418: 1) a secularly varying pattern of cool spots on the secondary; and 2) inhomogeneous co-orbiting clouds ejected from the primary.

ad 1) The mass of the secondary component was derived by Božić et al. (2007) to be 1.09 $M_\odot$. We suppose that a synchronously and therefore very quickly rotating star with a thick convective envelope is covered by cool dark spots which may make up a substantial part of the star. The coverage of the surface changes on a time scale from weeks to decades.

However, we argue that the light variations evoked by the spottiness of the secondary cannot explain the seasonal variability of HD 143418 because of the relative faintness of the secondary with respect to the primary. Provided that the luminosity ratio in V: $L_2^V/L_{\rm tot}^V = 0.06(2)$ (Božić et al. 2007), the contribution of the secondary to the magnitude of the binary in V is only −0.063(21) mag, −0.043 mag in B, and −0.045 mag in U. These contributions are comparable with the amplitudes of the variations (see Table 2, era III) which means, that the secondary would have to be completely extinct in some seasons. Moreover, in such a case the spectral lines of the secondary would not be visible in the observed spectrum.

ad 2) The process of spinning up of the primary described in Sect. 5.2.3 is obviously not uniform because the tidal interaction effectively affects mainly the outer parts of the star. The inner parts may rotate slower. This differential rotation of the stellar interior produces instabilities and eddies, leading to ejection of material from the star. This could be the origin of the observed seasonal light variations of the system. Some of that ejected material orbits around the centre of mass and reflects or obscures the primary component. As the parameter α has a reasonable probability of being positive, obscuring seems to prevail over reflection.

The absence of emission lines in the spectrum and the observed constancy of amplitudes of light variations represent very strong constraints on the state of the ejected co-orbiting matter. The only interaction between the light and matter, which is absolutely grey, is light scattering on free electrons or extinction and reflection on large dust particles. In the case of Thomson scattering on free electrons, a cloud of a cross section of about $100\,R_\odot^2$ and mass of $1.5 \times 10^{-11}\,M_\odot$ is sufficient to explane of the observed seasonal light variations. In the case of extinction and reflection on dust particles of 10^{-4} m in diameter amounting to

$\cong$1% of the mass of the cloud, we need only 5×10^{-12} $M_\odot$. For the ejection of such a cloud we need only a 10^{-8} portion of the total dissipated energy $E_{\rm diss}$ given by Eq. (11).

5.4. Short-time variability

Residuals of light curves after subtracting the above discussed persistent and seasonal changes exhibit relatively large scatter evoking the possibility of a specific short-time scale variability resembling flickering. However, the detailed statistical analysis of the residuals indicates that the observed scatter is caused by random observational errors rather then true short-time scale light variability such as flickering.

6. Conclusions

We analysed 23 time series Coudé spectra to investigate possible spectrum variations of the CP-candidate star HD 143418. Equivalent widths of 25 unblended lines of iron, chromium, titanium, zirconium and barium change within less than 2σ of their mean values, which reflects the accuracy of measurements. We examined spectral lines of different Lande factors on spectra acquired with a Zeeman analyser. The left and right circularly polarised profiles of the lines are identic, suggesting either absence of the global magnetic field or that the spectra were taken in rare moments when an alternating field acquired its zero value. The abundance pattern of the primary component derived from the Zeeman as well as from a wide region echelle spectrum does not correspond to any of the CP-types stars. The only possible peculiarity is the deficit of scandium which, however, is one of the characteristics of invariable Am-type stars.

We confirmed the extremely subsynchronous rotation of the primary component and argue that the star may be passing through its fast period of synchronisation.

By analysing intensities of spectral lines of carbon and silicon, we found a dichotomy in their behaviour manifested by the occurence of two groups of lines showing two remarkably different abundances. We stress the strong need for further improvement of atomic data for these elements.

Our, as well as previous findings, offer an inconsistent picture of HD 143418. There are at least two directions in which investigations of HD 143418 should continue, namely to confirm or rule out its magnetic field, and to identify the source of the seasonal photometric variations.

Acknowledgements. We thank P. Harmanec and M. Wolf for calling our attention to this interesting subject of investigation and inspiring discussion, J. Budaj for fruitful discussions, and T. Ryabchikova for discussion on *gf*-values. Our thanks go to the referee Dr. H. Hensberge whose comments, recommendations and advice helped to notably improve this paper. Partial support of grants VEGA 2/0074/9, GAAV IAA301630901, APVV SK-CZ-0090-07, Russian FBR 09-02-00002-a, and Bulgarian NSF NIK-05 and DO02-85(CVP01/002) is acknowledged.

References

Adelman, S. J., Malanushenko, V., Ryabchikova, T. A., et al. 2001, A&A, 375, 982
Asplund, M., Grevesse, N., & Sauval, A. J. 2005, in Cosmic Abundances as Records of Stellar Evolution and Nucleosynthesis, ed. T. G. Barnes III, & F. N. Bash (San Francisco: ASP), ASP Conf. Ser., 336, 25
Bagnulo, S., Jehin, E., Ledoux, C., et al. 2003, The Messenger, 114, 10, and www.sc.eso.org/santiago/uvespop/
Bartaya, R. A. 1979, Bull. Abastumani Astrophys. Obs., No. 51, 1
Božić, H., Wolf, M., Harmanec, et al. 2007, A&A, 464, 263
Budaj, J. 1996, A&A, 313, 523
Budaj, J. 1997, A&A, 326, 655
Budaj, J. 1999, MNRAS, 310, 419
Budaj, J., & Komžík, R. 2000, http://www.ta3.sk/~budaj/software
Castelli, F., & Kurucz, R. L. 2003, IAU Symp. 210, ed. N. Piskunov, W. W. Weiss, & D. F. Gray (San Francisco), ASP Conf. Ser., 20, http://www.user.oat.ts.astro.it/castelli/
Claret, A., Gimenez, A., & Cunha, N. C. S. 1995, A&A, 299, 724
ESA 1997, in The Hipparcos and Tycho Catalogues, ESA SP-1200, Noordwijk
Frémat, Y., Lampens, P., & Hensberge, H. 2005, MNRAS, 356, 545
Garz, T. 1973, A&A, 26, 471
Griffin, R. E. 2002, AJ, 123, 988
Griffin, R. E. M. 2004, in The A-Star Puzzle, ed. J. Zverko, J. Žižňovský, S. J. Adelman, & W. W. Weiss (Cambridge: Cambridge Univ. Press), IAU Symp., 224, 562
Griffin, R. E. M. 2008, CoSka, 38, 93
Hubeny, I., Lanz, T., & Jeffery, C. S. 1994, Newsletter on analysis of astronomical spectra, No. 20, ed. C. S. Jeffery, CCP7 (St. Andrews: St. Andrews Univ.), 30
Khaliullin, Kh. F., & Khaliullina, A. I. 2007, MNRAS, 382, 356
Krtička, J. 1998, Thesis, Masaryk University, Brno, in Czech language
Krtička, J., Mikulášek, Z., Henry, G. W., et al. 2009 A&A, 449, 567
Kudryavtsev, D. O. 2000, Baltic Astron., 9, 649
Kupka, F., Piskunov, N. E., Ryabchikova, T. A., Stempels, H. C., & Weiss, W. W. 1999, A&AS, 138, 119
Kupka, F., Ryabchikova, T. A., Piskunov, N. E., Stempels, H. C., & Weiss, W. W. 2000, Baltic Astron., 9, 590
Kurucz, R. L., & Bell, B. 1995, CD ROM 23, http://kurucz.harvard.edu/linelists.html
Kurucz, R. L., & Peytremann, E. 1975, SAO Spec. Report, 362
Lambert, D. L., & Luck, R. E. 1978, MNRAS, 183, 79
Lenz, P., & Breger, M. 2005, CoAst, 146, 53
Mathys, G., Hubrig, S., Landstreet, J. D., Lanz, T., & Manfroid, J. 1997, A&AS, 123, 353
Meynet, G., & Meader, A. 2006, in Stars with the B[e] Phenomenon, ed. M. Kraus, & A. S. Miroshnichenko, ASP Conf. Ser., 355, 27
Mikulášek, Z. 2007, Astron. Astrophys. Trans., 26(1), 63
Mikulášek, Z., Zverko, J., Romanyuk, I. I., et al. 2004, in Magnetic stars, ed. Yu. V. Glagolevskij, D. O. Kudryavtsev, & I. I. Romanyuk, Special Astrophys. Obs., Nizhnij Arkhyz, 191
Mikulášek, Z., Krtička, J., Zverko, J., et al. 2007a, in Physics of Magnetic Stars, ed. I. I. Romanyuk, & D. O. Kudryavtsev, Special Astrophys. Obs., Nizhnij Arkhyz, 300
Mikulášek, Z., Janík, J., Zverko, J., et al. 2007b, AN, 328, 10
Mikulášek, Z., Krtička, J., Henry, G. W., et al. 2008, A&A, 485, 585
North P. 1994, in Workshop and Meeting of EWG on CP Stars, ed. I. Jankovics, & I. J. Wincze, 53
North, P., Ginestet, N., Carquillat, J.-M., Carrier, F., & Udry, S. 1998, CoSka, 27, 179
Panchuk, V. E. 1998, SAO technical Report, N258
Panchuk, V. E., Piskunov, N. E., Klochkova, V. G., Yushkin, M. V., & Ermakov, S. V. 2002, SAO Preprint, N169
Piskunov, N. E., Kupka, F., Ryabchikova, T. A., Weiss, W. W., & Jeffery, C. S. 1995, A&AS, 112, 525
Polosukhina, N., Kurtz, D., Hack, M. et al. 1999, A&A, 351, 283
Popper, D. M. 1984, AJ, 89, 1057
Preston, G. W. 1974, ARA&A, 12, 257
Ralchenko, Yu., Kramida, A. E., Reader, J., & NIST ASD Team (2008), NIST Atomic Spectra Database (version 3.1.5), [Online], available: http://physics.nist.gov/asd3 [2009, March 4], National Institute of Standards and Technology, Gaithersburg, MD
Romanyuk, I. I. 2004, in Magnetic stars, ed. Yu. V. Glagolevskij, D. O. Kudryavtsev, & I. I. Romanyuk, Special Astrophys. Obs., Nizhnij Arkhyz, 33
Ryabchikova, T. A., Piskunov, N. E., Kupka, F., et al. 1997, Baltic Astron., 6, 244
Shore, S. N., & Adelman, S. J. 1976, ApJ, 209, 813
Tassoul, M., & Tassoul, J.-L. 1988, MNRAS, 232, 481
Wolff, S. C. 1983, NASA SP-463, 42
Zverko, J., Žižňovský, J., & North, P. 1998, CoSka, 28, 109
Zverko, J., Žižňovský, J., Mikulášek, Z., et al. 2007, CoSka, 37, 49
Žižňovský, J., Schwartz, P., & Zverko, J. 2000, IBVS, 4835

Table 5. List of lines used in abundance determination using the Zeeman spectrum.

Ion	Abund. factor	Line Å	*EP* eV	log *gf*	Notes
Mg I	vW 1.0	4571.096	0.000	–5.691	
Mg II	M 1.0	4390.572	9.999	–0.530	blend
	vW 1.0	4427.994	9.996	–1.210	
	W 1.0	4433.988	9.999	–0.910	
	vS 2.0	4481.1-3	8.864	0.740	triplet
Si I	0.03	4392.560	4.930	–1.920	MIO
	0.03	4448.792	4.930	–3.650	MIO
	0.03	4487.688	4.954	–2.220	MIO
	0.03	4505.931	4.954	–2.150	MIO
	0.03	4551.812	5.082	–3.500	MIO
	0.03	4601.257	5.082	–2.120	MIO
	0.03	4627.383	5.082	–1.520	MIO
Si II	0.03	4621.418	12.525	–0.540	MIO
	0.03	4621.722	12.526	–0.380	MIO
S I	0.3	4429.142	6.860	–1.900	MIO
	0.3	4431.435	6.860	–1.900	MIO
Ca I	M 1.0	4425.437	1.879	–0.286	KB95
	S 1.0	4434.957	1.886	0.066	KB95
	M 1.0	4435.679	1.886	–0.412	KB95
	M 1.0	4455.887	1.899	–0.414	KB95
	vW 1.0	4456.616	1.899	–1.590	KB95
	W 1.0	4578.551	2.521	–0.170	KB95
	W 1.0	4581.395	2.523	0.000	KB95, blend
	W 1.0	4585.865	2.526	0.161	KB95
	S 1.0	4454.779	1.899	0.335	KB95
Ca II	W 1.0	4472.053	6.468	–1.634	KP75
	W 1.0	4479.433	6.468	–1.935	KP75
Sc II	M 0.075	4400.389	0.605	–0.536	
	M 0.075	4415.557	0.595	–0.668	
	vW 0.075	4420.669	0.619	–2.273	
	vW 0.075	4431.352	0.605	–1.969	
Ti I	vW 2.0	4449.143	1.887	0.500	
	W 2.0	4533.241	0.848	0.476	
	vW 2.0	4534.776	0.836	0.280	
Ti II	W 2.0	4391.031	1.231	–2.240	
	M 2.0	4394.051	1.221	–1.770	
	vS 2.0	4395.033	1.084	–0.510	
	M 2.0	4395.850	1.243	–1.970	
	S 2.0	4399.772	1.237	–1.220	
	W 1.0	4409.243	1.243	–2.290	blend
	M 2.0	4411.074	3.095	–0.670	
	W 2.0	4411.925	1.224	–2.550	
	S 2.0	4417.719	1.165	–1.230	
	M 2.0	4418.330	1.237	–1.990	
	W 2.0	4421.938	2.610	–1.580	
	W 2.0	4441.734	1.180	–2.270	
	vS 2.0	4443.794	1.080	–0.700	
	W 2.0	4444.558	1.116	–2.210	
	S 2.0	4450.482	1.084	–1.510	
Ti II	M 2.0	4464.450	1.161	–1.810	
	vS 2.0	4468.507	1.131	–0.600	
	M 2.0	4488.331	3.124	–0.510	
	vW 2.0	4493.513	1.080	–2.830	
	vW 2.0	4500.353	1.084	–3.340	
	vS 2.0	4501.273	1.116	–0.760	
	W 2.0	4518.327	1.080	–2.640	

Table 5. continued.

Ion	Abund. factor	Line Å	*EP* eV	log *gf*	Notes
	M 2.0	4524.687	1.231	–2.111	DNF
	M 2.0	4529.474	1.572	–1.650	
	vS 2.0	4533.969	1.237	–0.540	
	W 2.0	4544.028	1.243	–2.530	
	W 2.0	4545.133	1.131	–2.460	
	S 2.0	4563.761	1.221	–0.790	
	vW 2.0	4568.314	1.224	–2.65	KB95
	vS 2.0	4571.968	1.572	–0.230	
Cr I	W 1.0	4540.488	2.544	–2.515	
	W 1.0	4540.734	3.104	0.028	
	W 1.0	4545.945	0.941	–1.370	
	vW 1.0	4600.741	1.004	–1.260	
	vW 1.0	4622.453	3.551	–0.040	
Cr II	W 1.0	4539.595	4.042	–2.290	
	M 1.0	4554.988	4.071	–1.281	
	vS 1.0	4558.650	4.073	–0.449	
	W 1.0	4565.740	4.042	–1.820	
	S 1.0	4588.199	4.071	–0.627	
	M 1.0	4592.049	4.074	–1.221	
	M 1.0	4616.629	4.072	–1.361	
	M 1.0	4618.803	4.074	–1.110	KB95
Fe I	vS 1.0	4404.750	1.557	–0.142	
	W 1.0	4408.413	2.198	–1.775	
	S 1.0	4415.123	1.608	–0.615	
	M 1.0	4427.310	0.052	–2.924	blend
	W 1.0	4430.614	2.223	–1.659	
	W 1.0	4433.219	3.654	–0.700	
	M 1.0	4442.339	2.198	–1.255	
	vW 1.0	4446.832	3.686	–1.320	
	M 1.0	4447.717	2.223	–1.342	
	M 1.0	4459.118	2.176	–1.279	
	M 1.0	4466.552	2.831	–0.600	
	M 1.0	4476.019	2.845	–0.819	blend
	M 1.0	4482.253	2.223	–1.482	blend
	vW 1.0	4482.739	3.654	–1.350	
	M 1.0	4484.220	3.602	–0.720	KB95
	W 1.0	4485.676	3.686	–1.020	
	vW 1.0	4490.084	3.017	–1.580	
	vW 1.0	4490.762	3.943	–1.158	blend
	M 1.0	4494.563	2.198	–1.136	
	vW 1.0	4517.525	3.071	–1.858	
	W 1.0	4531.148	1.485	–2.155	
	W 1.0	4547.847	3.546	–0.780	KB95
	vW 1.0	4560.088	3.602	–1.920	
	vW 1.0	4587.128	3.573	–1.737	
	vW 1.0	4598.117	3.283	–1.570	
	vW 1.0	4602.001	1.608	–3.154	
	W 1.0	4602.941	1.485	–2.209	
	W 1.0	4607.647	3.266	–1.545	
	W 1.0	4611.284	3.654	–0.670	KB95
Fe I	W 1.0	4625.045	3.241	–1.340	
Fe II	W 1.0	4413.601	2.676	–3.870	KB95
	S 1.0	4416.830	2.778	–2.600	KB95
	vW 1.0	4446.237	5.956	–2.439	
	W 1.0	4472.929	2.844	–3.430	
	S 1.0	4491.405	2.856	–2.89	KP75
	S 1.0	4508.288	2.856	–2.41	KP75
	S 1.0	4515.339	2.844	–2.450	
	S 1.0	4520.224	2.807	–2.600	
	S 1.0	4522.634	2.844	–2.030	
	M 1.0	4541.524	2.856	–3.050	KB95

Table 5. continued

Ion	Abund. factor	Line Å	*EP* eV	log *gf*	Notes
	S 1.0	4555.893	2.828	–2.160	
	M 1.0	4576.340	2.844	–2.920	
	M 1.0	4582.835	2.844	–3.090	
	vS 1.0	4583.837	2.807	–1.860	blend
	vW 1.0	4601.378	2.891	–4.428	
	M 1.0	4620.521	2.828	–3.29	NIST
Ni I	W 1.0	4546.920	4.165	–0.271	
	W 1.0	4604.982	3.480	–0.250	
Zr II	W 1.5	4440.452	1.208	–1.127	
	W 1.5	4443.008	1.486	–0.330	
	W 1.5	4457.431	1.840	–0.800	
	W 1.5	4496.980	0.713	–0.860	
Ba II	S 2.5	4554.029	0.000	0.170	

Note: Symbols in the second column indicate line stregth: vW = very weak, W = weak, M = medium, S = strong, vS = very strong. In the last column the source of the *gf*-value is given when other than VALD values are used. DNF = does not fit with either *gf*-value; MIO = missing in the observed spectrum; blend = two lines of the same species.

Table 6. List of lines used in abundance determination using the echelle spectrum.

Ion	Abund. factor	Line Å	*EP* eV	log *gf*	Notes
C I	vW 1.0	4734.256	7.946	–2.366	
	vW 1.0	4738.214	7.946	–3.115	
	vW 1.0	4738.461	7.946	–2.638	
	vW 1.0	4742.561	7.946	–2.990	
	vW 1.0	4766.672	7.483	–2.617	
	W 1.0	4770.026	7.483	–2.439	
	S 1.0	4771.742	7.488	–1.866	
	W 1.0	4775.895	7.488	–2.304	
	1.0	4795.860	7.946	–1.020	MIO
	M 1.0	4812.920	7.480	–3.377	
	vW 1.0	4817.373	7.483	–3.039	
	vW 1.0	4826.791	7.488	–3.182	
	M 1.0	4932.049	7.685	–1.884	
	vW 1.0	5017.091	7.946	–2.456	
	W 1.0	5023.839	7.946	–2.209	
	vW 1.0	5024.916	7.946	–2.728	
	M 1.0	5039.057	7.946	–2.000	KB95
	vW 1.0	5039.100	7.946	–2.286	
	W 1.0	5040.125	7.946	–2.303	
	S 1.0	5052.167	7.685	–1.303	NIST
	vW 1.0	5059.656	8.537	–2.480	
	vW 1.0	5295.426	8.537	–2.810	
	vW 1.0	5299.973	8.647	–2.550	
	M 1.0	5306.830	8.643	–2.290	KB95
	M 1.0	5380.337	8.851	–1.840	blend
	vW 1.0	5430.920	8.848	–2.410	
	vW 1.0	5545.050	8.640	–2.376	blend
	vW 1.0	5551.576	8.643	–2.030	KB95
	W 1.0	5793.120	7.946	–2.062	
	vW 1.0	5794.473	7.946	–2.790	
	vW 1.0	5800.602	7.946	–2.338	blend
	vW 1.0	5805.200	7.946	–2.682	blend
	vW 1.0	6001.118	8.643	–2.070	
	vW 1.0	6007.175	8.640	–2.180	KB95
	vW 1.0	6010.675	8.640	–2.020	KB95
	vW 1.0	6012.225	8.640	–2.300	KB95
	W 1.0	6014.830	8.643	–1.710	KB95
	vW 0.4	5693.109	8.537	–1.850	DNF
	M 0.4	6013.165	8.647	–1.314	DNF

Table 6. continued.

Ion	Abund. factor	Line Å	*EP* eV	log *gf*	Notes
	vW 0.02	4783.798	7.946	–2.560	
	0.02	4815.220	7.946	–2.130	MIO
	0.02	4815.475	7.946	–2.420	MIO
	0.02	4836.763	8.537	–2.610	MIO
	0.02	4921.419	8.537	–3.010	MIO
	0.02	4922.694	8.537	–2.630	MIO
	0.02	4926.427	8.537	–1.974	MIO
	0.02	4935.431	8.643	–2.690	MIO
	0.02	4940.609	8.537	–2.920	MIO
	0.02	4943.541	8.647	–2.460	MIO
	0.02	5018.068	7.946	–2.000	MIO
	vW 0.02	5155.098	8.647	–1.820	blend
	0.02	5159.919	8.643	–2.150	MIO
	0.02	5302.870	8.647	–1.840	MIO
	vW 0.02	5306.314	8.647	–1.874	
	0.02	5308.002	8.643	–2.750	MIO
	0.02	5374.341	8.848	–2.310	MIO
	vW 0.02	5436.872	8.851	–2.130	blend
	0.02	5515.551	8.851	–2.340	MIO
C I	0.02	5540.751	8.643	–2.376	MIO
	0.02	5547.267	8.640	–2.252	MIO
	0.02	5548.902	8.647	–1.760	MIO
	0.02	5551.018	8.647	–1.629	MIO
	0.02	5553.174	8.643	–2.370	MIO
	0.02	5603.724	8.771	–2.418	MIO
	0.02	5659.937	8.537	–1.960	MIO
	0.02	5758.579	9.003	–1.990	MIO
	0.02	5773.688	9.989	–1.310	MIO
	0.02	5812.718	8.851	–2.160	MIO
	0.02	5850.236	8.771	–2.290	MIO
	0.02	5877.341	8.771	–2.143	MIO
	0.02	6044.776	9.003	–2.071	MIO
	0.02	6107.659	8.851	–1.993	MIO
O I	0.2	4772.446	10.740	–2.269	MIO
	0.2	4773.755	10.741	–1.667	MIO
	0.2	4967.374	10.740	–1.977	MIO
	vW 1.0	5329.677	10.741	–2.063	NIST, blend
	W 1.0	5330.737	10.741	–1.570	NIST, blend
	vW 0.5	5435.178	10.740	–1.766	
	vW 0.5	5435.775	10.741	–1.544	
Na I	vW 0.9	4982.814	2.104	–0.950	blend
	vW 1.0	5148.839	2.012	–2.060	
	W 1.0	5682.633	2.012	–0.700	
	M 1.0	5688.205	2.104	–0.450	blend
Mg I	vS 1.0	5167.321	2.709	–1.030	
	vS 1.0	5172.684	2.712	–0.402	
	vS 1.0	5183.604	2.717	–0.180	
	S 1.0	5528.405	4.346	–0.620	
	W 1.0	5711.088	4.346	–1.833	
	vW 1.0	5785.313	5.108	–2.110	
	vW 1.0	5785.561	5.108	–2.500	
	vW 1.0	5785.672	5.108	–2.810	
Mg II	0.3	4739.593	11.569	–0.660	MIO
	0.3	4739.709	11.569	–0.820	MIO
	0.3	4851.099	11.630	–0.680	MIO
	vW 0.3	5401.556	11.630	–0.340	blend
Si I	0.8	4782.991	4.954	–2.229	MIO
	vW 0.8	5675.417	5.619	–1.231	
	W 0.8	5684.484	4.954	–1.732	

Table 6. continued.

Ion	Abund. factor	Line Å	*EP* eV	log *gf*	Notes
	vW 0.8	5690.425	4.930	–1.769	
	vW 0.8	5701.104	4.930	–1.581	–2.050, KB95
	W 0.8	5708.400	4.954	–1.034	–1.470, KB95
	vW 0.8	5747.667	5.614	–1.543	
	vW 0.8	5753.623	5.616	–1.754	–0.830, KB95
	vW 0.8	5772.146	5.082	–1.358	–1.750, KB95
	M 0.8	5948.541	5.082	–0.780	
	vW 0.8	6091.919	5.871	–1.470	
	vW 0.8	6125.021	5.614	–1.464	
	vW 0.8	6131.573	5.616	–2.393	
	vW 0.8	6131.852	5.616	–1.615	
	W 0.03	4792.213	4.930	–2.140	
	W 0.03	4792.324	4.954	–1.676	
	0.03	4947.607	5.082	–1.760	MIO
	S 0.03	5006.059	5.082	–1.296	
	0.03	5583.902	5.619	–1.464	MIO
Si I	vW 0.03	5665.555	4.920	–1.750	
	0.03	5721.021	5.863	–0.851	MIO
	0.03	5754.218	4.954	–1.842	MIO
	0.03	5761.507	5.863	–1.598	MIO
	0.03	5788.984	5.863	–1.272	MIO
	0.03	5803.559	5.616	–1.729	MIO
	0.03	5810.768	5.863	–1.469	MIO
	0.03	5813.081	5.619	–1.371	MIO
	0.03	5846.612	5.619	–1.832	MIO
	0.03	6037.079	5.964	–1.447	MIO
	0.03	6042.399	5.964	–1.309	–4.300 KB95 MIO
	0.03	6046.694	5.954	–0.935	MIO
	0.03	6047.516	5.984	–1.271	MIO
Si II	S 0.8	5055.984	10.074	0.593	
	W 0.8	5056.317	10.074	–0.359	
	W 0.8	5978.930	10.074	0.004	
S I	0.05	5696.966	7.866	–1.260	MIO
	0.05	5700.580	7.868	–1.040	MIO
	0.05	5706.424	7.870	–0.950	MIO
	0.05	5961.211	8.046	–1.200	MIO
Ca I	M 1.4	5261.704	2.521	–0.579	
	M 1.4	5264.237	2.523	–0.574	
	S 1.4	5265.556	2.523	–0.113	
	M 1.4	5349.465	2.709	–0.310	
	W 1.4	5512.980	2.933	–0.464	
	M 1.4	5581.965	2.523	–0.555	
	S 1.4	5588.749	2.526	0.358	
	M 1.4	5590.114	2.521	–0.571	
	S 1.4	5594.462	2.523	0.097	
	S 1.4	5598.480	2.521	–0.087	
	M 1.4	5601.277	2.526	–0.523	
	vW 1.4	5809.118	3.910	–1.073	blend
	S 1.4	5857.451	2.933	0.240	
	vW 1.4	5867.562	2.933	–1.570	
	M 1.4	6102.723	1.879	–0.793	
	S 1.4	6122.217	1.886	–0.316	
Ca II	W 1.4	4799.973	8.438	–2.013	–2.19, KP75
	W 1.4	4799.973	8.438	–0.499	–0.65, KP75
	W 1.4	4799.973	8.438	–0.582	–0.76, KP75
	M 1.4	5001.479	7.505	–0.507	
	S 1.4	5019.971	7.515	–0.247	
	W 1.4	5021.138	7.515	–1.207	
	W 1.4	5285.266	7.505	–1.147	
	M 1.4	5307.224	7.515	–0.848	

Table 6. continued.

Ion	Abund. factor	Line Å	*EP* eV	log *gf*	Notes
	M 1.4	5339.188	8.438	–0.334	
	1.4	5659.889	7.050	–3.838	MIO
	vW 1.4	5748.374	8.763	–0.978	
Sc II	S 0.075	5031.021	1.357	–0.400	
	M 0.075	5239.813	1.455	–0.765	
	vW 0.075	5318.349	1.357	–2.015	
	vW 0.075	5357.199	1.507	–2.111	
	S 0.075	5526.790	1.768	0.024	
	vW 0.075	5641.001	1.500	–1.131	
	M 0.075	5657.896	1.507	–0.600	
	M 0.075	5658.361	1.500	–1.210	
Sc II	vW 0.075	5667.149	1.500	–1.309	
	W 0.075	5684.202	1.507	–1.074	
Ti I	vW 2.1	4758.118	2.249	0.425	
	vW 2.1	4759.270	2.256	0.514	
	vW 2.1	4820.411	1.502	–1.441	
	vW 2.1	4870.126	2.249	0.518	
	vW 2.1	4885.079	1.887	0.358	
	vW 2.1	4913.614	1.873	0.160	
	vW 2.1	4928.336	2.154	0.050	
	vW 2.1	4975.342	2.506	–0.001	
	M 2.1	4981.731	0.848	0.504	
	W 2.1	4999.503	0.826	0.250	
	W 2.1	5014.276	0.813	0.047	
	vW 2.1	5025.570	2.041	0.250	
	vW 2.1	5064.653	0.048	–0.991	
	vW 2.1	5124.072	1.502	–0.082–	–0.99, KP75
	vW 2.1	5173.743	0.000	–1.118	
	vW 2.1	5192.969	0.021	–1.006	
	vW 2.1	5210.385	0.048	–0.884	
Ti II	M 2.1	4763.881	1.221	–2.360	
	S 2.1	4779.985	2.048	–1.260	
	W 2.1	4798.521	1.080	–2.680	
	vS 2.1	4805.085	2.061	–0.960	
	vW 2.1	4806.321	1.084	–3.761	
	vW 2.1	4849.169	1.131	–3.000	
	vW 2.1	4855.905	3.095	–1.470	
	vW 2.1	4865.611	1.116	–2.790	
	M 2.1	4874.010	3.095	–0.800	
	S 2.1	4911.193	3.124	–0.610	
	M 2.1	4981.355	1.566	–3.200	
	vW 2.1	4996.367	1.582	–2.915	KB95
	vW 2.1	5005.157	1.566	–2.720	
	W 2.1	5010.211	3.095	–1.290	
	vW 2.1	5013.330	3.095	–1.910	
	M 2.1	5013.677	1.582	–2.190	
	vW 2.1	5069.090	3.124	–1.390	KB95
	S 2.1	5129.152	1.892	–1.240	
	S 2.1	5154.068	1.566	–1.750	
	S 2.1	5185.902	1.893	–1.35	KP75
	M 2.1	5211.530	2.590	–1.356	KB95
	vW 2.1	5252.019	2.590	–2.502	KB95
	S 2.1	5336.771	1.582	–1.590	
	M 2.1	5381.015	1.566	–1.920	
	vW 2.1	5396.226	1.584	–2.925	KB95
	vW 2.1	5396.558	2.598	–1.770	DNF
	M 2.1	5418.751	1.582	–1.999	
	W 2.1	5490.690	1.566	–2.650	KB95
	vW 2.1	5492.862	1.582	–2.956	KB95
V II	vW 1.0	4746.386	2.372	–1.749	-2.01, KP75
	vW 1.0	4883.407	3.796	–0.778	-0.93, KP75

Table 6. continued.

Ion	Abund. factor	Line Å	*EP* eV	log *gf*	Notes
	1.0	4965.409	3.799	–1.043	MIO
	1.0	5047.290	2.557	–2.088	MIO
	1.0	5241.164	4.516	–0.689	MIO
	vW 1.0	5303.255	2.276	–1.936	
	vW 1.0	5819.935	2.522	–1.703	–1.98, KP75
	vW 1.0	5928.862	2.522	–1.598	
Cr I	vW 1.0	4737.347	3.087	–0.099	
	vW 1.0	4752.087	4.186	0.440	
	W 1.0	4756.112	3.104	0.090	
	W 1.0	4789.335	2.544	–0.366	
	vW 1.0	4801.025	3.122	–0.131	
	vW 1.0	4829.371	2.545	–0.810	
	W 1.0	4870.797	3.079	0.050	
	W 1.0	4922.265	3.104	0.270	
	vW 1.0	4936.336	3.113	–0.340	
	S 1.0	5204.511	0.941	–0.208	
	S 1.0	5206.037	0.941	0.019	
	S 1.0	5208.425	0.941	0.158	
	vW 1.0	5247.565	0.961	–1.640	
	W 1.0	5296.691	0.983	–1.400	
	W 1.0	5297.377	2.900	0.167	
	W 1.0	5298.272	0.983	–1.150	blend
	W 1.0	5345.796	1.004	–0.980	
	W 1.0	5348.315	1.004	–1.290	
	M 1.0	5409.784	1.030	–0.720	
	vW 1.0	5787.918	3.322	–0.083	
	W 1.0	5790.957	3.321	0.324	
Cr II	M 1.0	4812.337	3.864	–1.960	
	vS 1.0	4824.127	3.871	–1.085	
	M 1.0	4836.229	3.858	–2.042	
	S 1.0	4848.235	3.864	–1.280	
	W 1.0	4856.186	3.854	–2.181	
	M 1.0	4864.326	3.858	–1.470	
	S 1.0	4876.399	3.854	–1.580	blend
	M 1.0	4884.607	3.858	–2.231	
	vW 1.0	4901.623	6.487	–1.141	
	vW 1.0	4912.462	6.484	–1.262	
	W 1.0	5153.498	3.758	–2.500	
	vW 1.0	5210.865	3.758	–2.941	
	S 1.0	5237.329	4.037	–1.350	
	W 1.0	5246.768	3.714	–2.560	
	W 1.0	5249.437	3.758	–2.752	
	S 1.0	5274.964	4.071	–1.559	
	M 1.0	5305.853	3.827	–2.160	
	M 1.0	5308.408	4.071	–0.058	
	W 1.0	5310.686	4.072	–2.408	
	M 1.0	5313.563	4.074	–1.779	
	vW 1.0	5318.382	3.714	–3.225	
	M 1.0	5334.869	4.072	–1.826	
	vW 1.0	5346.538	3.758	–3.095	
	W 1.0	5407.604	3.827	–2.459	
	W 1.0	5420.922	3.758	–2.558	
	M 1.0	5478.365	4.178	–1.968	
	W 1.0	5502.067	4.168	–2.117	
	W 1.0	5503.212	4.143	–2.372	
	W 1.0	5508.606	4.156	–2.252	
	W 1.0	5510.702	3.827	–2.618	
	vW 1.0	6053.466	4.754	–2.219	
	vW 1.0	6089.632	6.487	–1.445	
Mn I	vW 1.5	4739.087	2.941	–0.490	
	M 1.5	4754.042	2.282	–0.086	
	vW 1.5	4761.512	2.953	–0.320	
	vW 1.5	4765.846	2.941	–0.080	

Table 6. continued.

Ion	Abund. factor	Line Å	*EP* eV	log *gf*	Notes
	W 1.5	4766.418	2.920	0.100	
Mn I	M 1.5	4783.427	1.298	0.042	
	M 1.5	4823.524	2.319	0.144	
	vW 1.5	5377.637	3.844	–0.109	
	vW 1.5	5399.499	3.853	–0.287	
	1.5	5420.355	2.143	–1.700	KP75, MIO
	1.5	5470.637	2.164	–1.702	–1.94, KP75, MIO
	vW1.5	6013.513	3.072	–0.251	
	W1.5	6021.819	3.075	0.034	
Mn II	vW 1.5	4755.727	5.397	–1.242	
	vW 1.5	5559.047	6.185	–1.318	
	vW 1.5	5570.539	6.177	–1.444	
	vW 1.5	5578.126	6.186	–1.400	
Fe I	vW 1.0	4733.591	1.485	–2.71	KB95
	W 1.0	4735.843	4.076	–1.325	-0.43, KP75
	M 1.0	4736.772	3.211	–0.752	
	vW 1.0	4737.635	3.267	–2.247	
	W 1.0	4741.529	2.831	–1.765	
	W 1.0	4745.800	3.645	–1.270	
	vW 1.0	4757.578	3.274	–2.040	
	W 1.0	4768.320	3.686	–1.070	
	W 1.0	4772.803	1.557	–2.897	–3.15, KP75
	vW 1.0	4772.830	3.017	–2.192	–2.42, KP75
	vW 1.0	4776.376	4.559	–1.301	
	vW 1.0	4779.439	3.415	–2.020	
	W 1.0	4786.806	3.017	–1.606	
	vW 1.0	4787.827	2.998	–2.530	
	W 1.0	4788.751	3.237	–1.763	
	M 1.0	4789.651	3.546	–0.958	
	vW 1.0	4800.649	4.143	–1.029	
	vW 1.0	4801.773	4.835	–1.236	
	W 1.0	4802.880	3.642	–1.514	
	vW 1.0	4832.728	3.640	–1.733	
	vW 1.0	4839.544	3.267	–1.822	
	vW 1.0	4843.143	3.396	–1.840	
	S 1.0	4872.136	2.882	–0.567	
	W 1.0	4881.718	3.301	–1.781	
	W 1.0	4882.143	3.417	–1.640	
	W 1.0	4885.430	3.882	–0.917	
	W 1.0	4886.332	4.154	–0.612	
	vW 1.0	4888.166	4.559	–1.013	MIO
	S 1.0	4890.754	2.875	–0.394	
	vW 1.0	4902.233	4.559	–1.382	MIO
	S 1.0	4891.492	2.851	–0.112	
	vW 1.0	4892.859	4.217	–1.290	
	S 1.0	4903.308	2.882	–0.926	
	vW 1.0	4905.133	3.928	–2.050	
	vW 1.0	4907.732	3.403	–1.840	
	vW 1.0	4909.383	3.929	–1.231	
	W 1.0	4910.017	3.397	–1.408	–1.647, KB95
	W 1.0	4910.325	4.191	–0.459	–0.92, KP75
	W 1.0	4910.565	4.218	–0.433	–0.84, KP75
	vW 1.0	4917.229	4.191	–1.15	KP75
	vW 1.0	4918.013	4.230	–1.360	
	S 1.0	4918.993	2.865	–0.342	
	S 1.0	4920.502	2.832	–2.616	
	W 1.0	4924.770	2.279	–2.241	
	W 1.0	4930.315	3.960	–1.201	
	W 1.0	4933.341	4.231	–0.817	
Fe I	W 1.0	4938.174	3.943	–0.906	
	M 1.0	4938.813	2.875	–1.077	

Table 6. continued.

Ion	Abund. factor	Line Å	*EP* eV	log *gf*	Notes
	W 1.0	4939.241	4.154	–0.829	
	vW 1.0	4939.686	0.859	–3.340	
	W 1.0	4946.385	3.368	–1.170	
	vW 1.0	4950.104	3.417	–1.670	
	S 1.0	4957.298	2.851	–0.408	
	S 1.0	4957.596	2.808	0.233	blend
	vW 1.0	4962.572	4.178	–1.182	
	M 1.0	4966.087	3.332	–0.871	
	M 1.0	4967.897	4.191	–0.487	
	vW 1.0	4968.392	4.220	–1.449	
	W 1.0	4969.916	4.217	–0.710	
	vW 1.0	4970.496	3.635	–1.740	
	W 1.0	4973.101	3.960	–0.950	KB95
	S 1.0	4982.499	4.103	0.156	–0.31, KP75
	M 1.0	4983.250	4.154	–0.122	
	M 1.0	4985.253	3.928	–0.560	
	M 1.0	4985.546	2.865	–1.332	
	vW 1.0	4986.223	4.217	–1.390	
	M	4988.945	4.154	–0.890	DNF
	W 1.0	4994.129	0.951	–3.080	
	vW 1.0	4999.113	4.186	–1.740	
	S 1.0	5005.712	3.884	0.029	–0.34, KP75
	S 1.0	5006.119	2.832	–0.87	KP75
	M 1.0	5012.067	0.859	–2.642	blend
	M 1.0	5014.941	3.943	–0.303	
	M 1.0	5022.236	3.984	–0.530	
	M 1.0	5027.123	4.154	–0.534	
	vW 1.0	5027.756	4.209	–1.250	
	W 1.0	5028.126	3.573	–1.123	
	vW 1.0	5044.210	2.851	–2.038	
	W 1.0	5048.433	3.960	–1.030	
	M 1.0	5049.819	2.279	–1.355	
	vW 1.0	5051.277	4.220	–1.107	–1.37, KP75
	M 1.0	5051.634	0.915	–2.795	
	vW 1.0	5060.036	4.301	–1.148	–1.41, KP75
	S 1.0	5065.018	4.256	0.005	
	W 1.0	5067.150	4.220	–0.970	
	M 1.0	5068.765	2.940	–1.042	
	W 1.0	5072.672	4.220	–0.837	
	M 1.0	5074.748	4.220	–0.200	–0.44, KP75
	vW 1.0	5075.172	4.178	–1.119	–1.58, KP75
	W 1.0	5076.264	4.301	–0.809	
	W 1.0	5079.739	0.990	–3.220	
	W 1.0	5083.338	0.958	–2.958	-2.64, KP75
	vW 1.0	5088.153	4.154	–1.780	
	M 1.0	5090.767	4.256	–0.400	
	M 1.0	5096.998	4.283	–0.268	
	M 1.0	5098.698	2.176	–2.026	blend
	vW 1.0	5108.397	4.559	–1.252	
	W 1.0	5109.650	4.301	–0.980	–0.66, KP75
	W 1.0	5110.358	3.573	–1.366	
	W 1.0	5110.413	0.000	–3.760	
	W 1.0	5121.639	4.283	–0.810	
	W 1.0	5123.719	1.011	–3.068	
	M 1.0	5125.112	4.220	–0.140	
	W 1.0	5126.192	4.256	–1.080	–0.92, KP75
	W 1.0	5127.358	0.951	–3.307	–3.02, KP75
	S 1.0	5133.681	4.178	0.140	
Fe I	S 1.0	5139.251	2.998	–0.741	
	S 1.0	5139.462	2.940	–0.509	
	W 1.0	5141.739	2.424	–2.150	KB95
	vW 1.0	5151.910	1.011	–3.322	
	W 1.0	5159.050	4.283	–0.820	
	S 1.0	5162.273	4.178	0.020	
	vW 1.0	5164.551	4.434	–1.360	

Table 6. continued.

Ion	Abund. factor	Line Å	*EP* eV	log *gf*	Notes
	M 1.0	5165.410	4.220	–0.003	–0.38, KP75
	M 1.0	5171.595	1.485	–1.793	
	vW 1.0	5187.914	4.143	–1.371	
	S 1.0	5191.454	3.038	–0.551	
	S 1.0	5192.343	2.998	–0.541	
	M 1.0	5194.941	1.557	–2.090	
	M 1.0	5195.472	4.220	–0.086	
	W 1.0	5196.059	4.256	–0.493	–0.89, KP75
	W 1.0	5198.711	2.223	–2.135	
	M 1.0	5202.335	2.176	–1.838	blend
	M 1.0	5215.179	3.266	–0.871	
	M 1.0	5216.274	1.608	–2.150	
	M 1.0	5217.389	3.211	–1.070	
	vW 1.0	5217.919	3.640	–1.709	
	vW 1.0	5223.183	3.635	–1.783	
	S 1.0	5226.862	3.038	–0.555	
	S 1.0	5227.150	2.242	–1.352	
	S 1.0	5227.189	1.557	–1.228	
	vW 1.0	5228.376	4.220	–1.290	–0.89, KP75
	M 1.0	5229.845	3.283	–0.967	–1.136, KB95
	M 1.0	5229.866	4.220	–0.310	–0.91, KP75
	S 1.0	5232.939	2.940	–0.058	
	W 1.0	5235.387	4.076	–0.854	
	vW 1.0	5236.202	4.186	–1.497	
	W 1.0	5242.491	3.634	–0.967	
	vW 1.0	5245.626	4.313	–0.567	MIO
	W 1.0	5250.645	2.198	–2.181	
	W 1.0	5253.461	3.283	–1.573	
	vW 1.0	5259.094	4.371	–0.711	MIO
	M 1.0	5263.305	3.266	–0.879	
	S 1.0	5266.555	2.998	–0.386	
	S 1.0	5269.537	0.859	–1.321	
	vW 1.0	5277.306	4.415	–1.049	MIO
	M 1.0	5281.790	3.038	–0.834	
	S 1.0	5283.621	3.241	–0.432	
	vW 1.0	5288.525	3.694	–1.508	
	vW 1.0	5292.597	4.991	–0.590	
	M 1.0	5302.299	3.283	–0.720	
	vW 1.0	5321.108	4.434	–0.951	
	S 1.0	5324.178	3.211	–0.103	
	W 1.0	5332.899	1.557	–2.777	
	M 1.0	5339.928	3.266	–0.647	
	M 1.0	5341.023	1.608	–1.953	
	W 1.0	5353.373	4.103	–0.840	
	M 1.0	5364.858	4.445	0.228	
	W 1.0	5365.399	3.573	–1.020	
	S 1.0	5367.466	4.415	0.443	
	S 1.0	5369.958	4.371	0.536	
	S 1.0	5371.489	0.958	–1.645	blend
	vW 1.0	5373.698	4.473	–0.860	
	vW 1.0	5379.574	3.694	–1.514	
	vW 1.0	5382.475	4.371	–0.975	–1.51, KP75
	S 1.0	5383.369	4.312	0.645	
Fe I	W 1.0	5389.479	4.415	–0.410	
	W 1.0	5391.459	4.154	–0.782	
	M 1.0	5393.167	3.241	–0.715	
	S 1.0	5397.127	0.915	–1.993	
	W 1.0	5398.277	4.445	–0.670	
	M 1.0	5400.501	4.371	–0.160	
	S 1.0	5404.117	4.313	0.247	
	S 1.0	5404.149	4.434	0.523	
	S 1.0	5405.774	0.990	–1.844	
	M 1.0	5410.910	4.437	0.398	

Table 6. continued.

Ion	Abund. factor	Line Å	*EP* eV	log *gf*	Notes
	S 1.0	5415.192	4.386	0.642	
	S 1.0	5424.068	4.320	0.520	
	S 1.0	5429.696	0.958	–1.789	blend
	M 1.0	5434.523	1.011	–2.122	
	M 1.0	5445.042	4.386	–0.020	
	S 1.0	5446.916	0.990	–1.914	
	S 1.0	5455.454	4.320	0.328	–0.19, KP75
	S 1.0	5455.609	1.011	–2.091	
	M 1.0	5462.960	4.437	–0.405	
	M 1.0	5463.271	4.434	0.110	
	vW 1.0	5464.280	4.143	–1.402	
	W 1.0	5466.390	4.371	–0.630	
	vW 1.0	5472.709	4.209	–1.495	
	W 1.0	5473.900	4.154	–0.760	
	W 1.0	5480.861	4.217	–1.260	
	W 1.0	5481.242	4.103	–1.243	
	M 1.0	5487.740	4.143	–0.710	
	M 1.0	5487.745	4.320	–0.317	–0.83, KP75
	W 1.0	5497.516	1.011	–2.849	
	W 1.0	5501.464	0.958	–3.040	
	W 1.0	5506.778	0.990	–2.797	
	vW 1.0	5522.446	4.209	–1.550	
	vW 1.0	5525.539	4.230	–1.084	
	vW 1.0	5543.147	3.695	–1.570	
	vW 1.0	5543.936	4.217	–1.140	
	W 1.0	5554.882	4.548	–0.440	
	vW 1.0	5560.207	4.434	–1.190	
	vW	5562.116	4.387	–0.439	MIO
	W 1.0	5562.706	4.435	–0.641	
	W 1.0	5565.704	4.608	–0.213	
	M 1.0	5569.618	3.417	–0.486	
	S 1.0	5572.841	3.396	–0.275	
	W 1.0	5576.089	3.430	–1.000	
	vW 1.0	5584.268	4.387	–0.991	–1.55, KP75
	S 1.0	5586.756	3.368	–0.120	
	S 1.0	5615.644	3.332	0.050	
	vW 1.0	5618.631	4.209	–1.276	
	M 1.0	5624.542	3.417	–0.755	
	W 1.0	5633.946	4.991	–0.270	
	W 1.0	5638.262	4.220	–0.870	
	vW 1.0	5641.434	4.256	–1.180	
	vW 1.0	5650.706	5.085	–0.960	
	W 1.0	5655.493	4.260	–0.796	blend
	W 1.0	5662.516	4.178	–0.573	
	vW 1.0	5667.518	4.178	–1.156	
	W 1.0	5679.023	4.652	–0.920	
	W 1.0	5686.530	4.548	–0.446	
	vW 1.0	5691.497	4.301	–1.520	
	W 1.0	5701.544	2.559	–2.216	
	vW 1.0	5705.464	4.301	–1.355	
Fe I	W 1.0	5709.378	3.368	–1.028	
	vW 1.0	5717.833	4.284	–1.130	
	vW 1.0	5731.762	4.256	–1.300	
	vW 1.0	5752.032	4.549	–1.177	
	W 1.0	5753.121	4.260	–0.688	
	M 1.0	5762.990	4.209	–0.450	
	vW 1.0	5775.081	4.220	–1.298	
	vW 1.0	5793.913	4.220	–1.700	
	vW 1.0	5798.169	3.928	–1.890	
	vW 1.0	5806.717	4.607	–1.050	
	W 1.0	5816.373	4.548	–0.601	
	vW 1.0	5834.025	4.913	–1.951	

Table 6. continued.

Ion	Abund. factor	Line Å	*EP* eV	log *gf*	Notes
	vW 1.0	5848.127	4.608	–1.056	
	vW 1.0	5852.217	4.548	–1.330	
	vW 1.0	5856.083	4.294	–1.328	
	W 1.0	5859.586	4.549	–0.419	
	M 1.0	5862.357	4.549	–0.127	
	W 1.0	6007.960	4.652	–0.957	
	W 1.0	6008.556	3.884	–0.986	
	W 1.0	6020.169	4.607	–4.170	
	M	6024.049	4.548	–0.120	DNF
	W 1.0	6027.051	4.076	–1.089	
	W 1.0	6055.992	4.733	–0.460	
	M 1.0	6065.482	2.608	–1.530	
	W 1.0	6078.491	4.796	–0.321	
	vW 1.0	6078.999	4.652	–1.120	
	vW 1.0	6127.906	4.143	–1.399	
	M 1.0	6136.615	2.453	–1.400	
Fe II	S 1.0	4731.453	2.891	–3.127	
	vW 1.0	4833.197	2.657	–4.795	
	W 1.0	4893.820	2.828	–4.267	
	vW 1.0	4913.292	10.288	0.050	
	vS 1.0	4923.927	2.890	–1.320	KB95
	vW 1.0	4948.096	10.308	–0.218	
	vW 1.0	4948.793	10.348	–0.031	
	vW 1.0	4951.656	10.308	0.311	
	vW 1.0	4953.987	5.571	–2.815	
	vW 1.0	4977.035	10.360	–0.039	
	vW 1.0	4984.488	10.329	0.078	
	vW 1.0	4990.509	10.329	0.195	
	M 1.0	4993.358	2.807	–3.684	
	vW 1.0	5000.743	2.778	–4.578	
	S 1.0	5001.959	10.273	0.916	
	W 1.0	5004.195	10.273	0.504	
	vW 1.0	5015.755	10.348	–0.028	
	vS 1.0	5018.440	2.891	–1.220	KB95
	W 1.0	5019.462	5.569	–2.784	
	vW 1.0	5030.630	10.288	0.431	
	vW 1.0	5032.712	10.392	0.077	
	vW 1.0	5045.114	10.308	–0.002	
	vW 1.0	5061.718	10.308	0.284	
	vW 1.0	5070.899	10.308	0.268	
	vW 1.0	5074.053	6.807	–2.170	
	vW 1.0	5089.214	10.329	0.013	
	vW 1.0	5093.575	10.379	0.166	blend
	M 1.0	5100.664	2.807	–4.197	blend
	vW 1.0	5117.034	10.430	–0.039	
	W 1.0	5120.352	2.828	–4.256	
	W 1.0	5127.866	5.571	–2.451	
Fe II	W 1.0	5132.669	2.080	–4.094	
	W 1.0	5136.802	2.844	–4.356	
	W 1.0	5146.127	2.828	–4.079	
	W 1.0	5149.465	10.448	0.544	
	W 1.0	5154.409	2.844	–4.269	
	W 1.0	5160.839	5.569	–2.559	
	vW 1.0	5161.184	2.856	–4.573	
	vS 1.0	5169.033	2.891	–0.870	KB95
	S 1.0	5197.577	3.230	–2.348	
	vW 1.0	5199.122	10.397	0.121	
	W 1.0	5216.863	10.480	0.670	
	S 1.0	5227.481	10.452	0.846	
	S 1.0	5234.625	3.221	–2.050	KB95
	vW 1.0	5247.952	10.531	0.500	
	vW 1.0	5251.233	10.520	0.424	
	M 1.0	5254.929	3.230	–3.336	
	W 1.0	5256.938	2.891	–4.182	

Table 6. continued.

Ion	Abund. factor	Line Å	*EP* eV	log *gf*	Notes
	M 1.0	5260.259	10.419	1.088	
	S 1.0	5264.812	3.230	–3.133	
	W 1.0	5272.397	5.956	–2.009	
	S 1.0	5276.002	3.199	–2.213	
	vW 1.0	5278.938	5.911	–2.677	
	S 1.0	5284.109	2.891	–3.195	
	W 1.0	5291.666	10.480	0.544	
	M 1.0	5325.553	3.221	–3.324	
	S 1.0	5362.869	3.199	–2.616	–2.739, KB95
	W 1.0	5387.063	10.522	0.499	
	W 1.0	5414.073	3.221	–3.645	
	M 1.0	5425.257	3.199	–3.390	
	W 1.0	5427.826	6.724	–1.581	
	vW 1.0	5465.931	10.623	0.348	
	W 1.0	5466.908	6.807	–1.873	
	vW 1.0	5482.308	10.562	0.413	
	W 1.0	5506.195	10.522	0.859	
	W 1.0	5525.125	3.627	–4.102	
	W 1.0	5529.932	6.792	–1.813	
	S 1.0	5534.847	3.245	–2.865	
	W 1.0	5567.842	6.730	–1.866	
	vW 1.0	5591.368	3.267	–4.590	
	vW 1.0	5627.497	3.387	–4.188	
	vW 1.0	5780.128	10.678	0.421	
	W 1.0	5813.677	5.571	–2.750	
	vW 1.0	5823.155	5.569	–2.987	
	vW 1.0	5835.492	5.911	–2.702	
	M 1.0	5991.376	3.153	–3.647	
	W 1.0	6084.111	3.199	–3.881	
	W 1.0	6113.322	3.322	–4.230	
Co I	vW 1.0	4813.467	3.216	0.050	
	vW 1.0	5342.695	4.021	0.690	
Ni I	vW 1.0	4732.456	4.105	–0.550	
	vW 1.0	4752.415	3.658	–0.700	
	vW 1.0	4754.756	3.635	–0.970	
	W 1.0	4756.510	3.480	–0.34	KB95
	W 1.0	4786.531	3.420	–0.160	–0.30, KP75
	vW 1.0	4817.815	4.154	–0.770	
	W 1.0	4829.016	3.542	–0.330	
	W 1.0	4831.169	3.606	–0.320	
	vW 1.0	4866.262	3.539	–0.210	
Ni I	vW 1.0	4873.438	3.699	–0.380	
	W 1.0	4904.407	3.542	–0.170	–0.05, KP75
	vW 1.0	4913.968	3.743	–0.630	
	W 1.0	4918.362	3.841	–0.240	
	vW 1.0	4925.577	3.655	–0.770	
	vW 1.0	4935.831	3.941	–0.350	
	vW 1.0	4937.341	3.606	–0.390	–1.22, KP75
	vW 1.0	4953.200	3.740	–0.670	KB95
	M 1.0	4980.166	3.606	0.070	
	vW 1.0	4996.841	3.635	–0.980	
	vW 1.0	4998.218	3.606	–0.690	
	W 1.0	5000.338	3.635	–0.430	
	vW 1.0	5010.934	3.635	–0.870	
	M 1.0	5017.568	3.539	–0.080	KB95
	M 1.0	5035.357	3.635	0.290	0.38 , KP75
	vW 1.0	5048.843	3.847	–0.380	
	M 1.0	5080.528	3.655	0.330	
	M 1.0	5081.107	3.847	0.300	
	W 1.0	5082.339	3.658	–0.540	

Table 6. continued.

Ion	Abund. factor	Line Å	*EP* eV	log *gf*	Notes
	W 1.0	5084.089	3.679	0.030	
	W 1.0	5099.927	3.679	–0.100	–0.21, KP75
	W 1.0	5115.389	3.834	–0.100	
	vW 1.0	5126.821	3.699	–0.702	–1.00, KP75
	W 1.0	5146.480	3.706	–0.060	
	W 1.0	5155.762	3.898	0.011	
	vW 1.0	5176.559	3.898	–0.440	
	vW 1.0	5625.312	4.089	–0.700	
	vW 1.0	5663.975	4.538	–0.430	
	vW 1.0	5694.977	4.089	–0.610	
	vW 1.0	5715.066	4.088	–0.352	
	vW 1.0	6086.276	4.266	–0.530	
Cu I	vW 0.2	5105.537	1.389	–1.516	
	vW 0.2	5153.230	3.786	0.217	
	W 0.2	5218.197	3.817	0.476	
	vW 0.2	5220.066	3.817	–0.448	
	vW 0.2	5782.127	1.642	–1.720	
Zn I	W 1.0	4810.528	4.078	–0.140	
Y II	W 1.8	4823.304	0.992	–1.110	
	M 1.8	4854.863	0.992	–0.380	
	S 1.8	4883.684	1.084	0.070	
	S 1.8	4900.120	1.033	–0.090	
	vW 1.8	4982.129	1.033	–1.290	
	M 1.8	5087.416	1.084	–0.170	
	vW 1.8	5119.112	0.992	–1.360	
	W 1.8	5123.211	0.992	–0.830	
	vW 1.8	5196.422	1.784	–0.880	–1.21, KP75
	W 1.8	5200.406	0.992	–0.570	
	M 1.8	5205.724	1.033	–0.340	
	vW 1.8	5289.815	1.033	–1.850	-2.24, KP75
	W 1.8	5402.774	1.839	–0.510	
	vW 1.8	5473.388	1.738	–1.020	
	W 1.8	5509.895	0.992	–1.010	
	vW 1.8	5546.009	1.748	–1.100	
	M 1.8	5662.925	1.944	0.160	
	vW 1.8	5781.689	1.839	–0.910	–1.28, KP75
Zr II	vW 2.5	5112.270	1.665	–0.850	
Ba II	S 4.0	4934.076	0.000	–0.150	
	W 1.9	5853.668	0.604	–1.000	

Note: Symbols in the second column indicates line stregth: vW = very weak, W = weak, M = medium, S = strong, vS = very strong. In the last column the source of the *gf*-value is given when other than VALD values are used. DNF = does not fit with either *gf*-value; MIO = missing in the observed spectrum; blend = two lines of the same species.

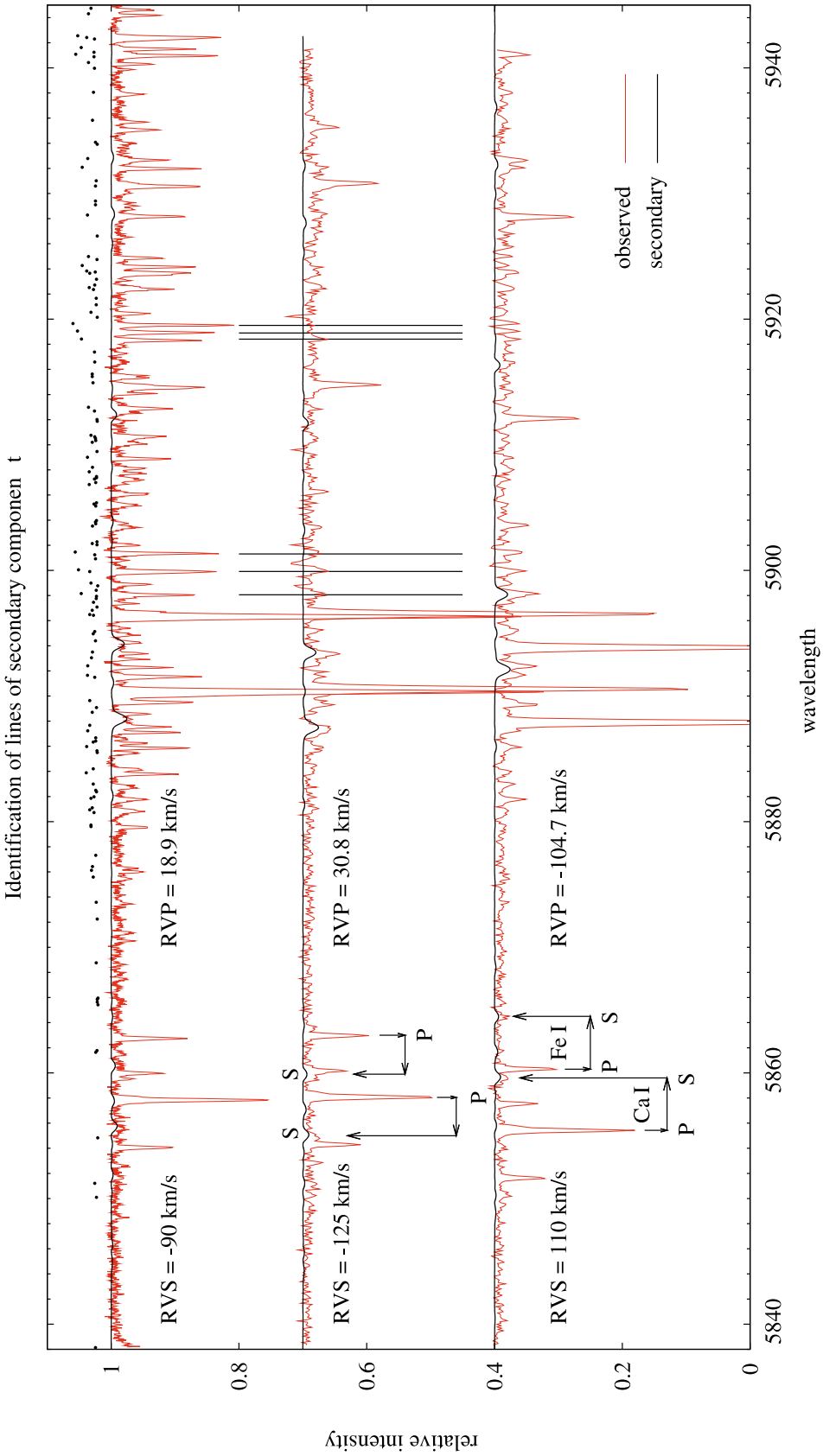

Fig. 14. Section of the spectrum around sodium D1D2 lines. *From top to bottom*: SAO echelle spectrum, phase 0.584, Rozhen Coudé spectra, phases 0.869 and 0.291. Mesured radial velocities of primary (RVP) and secondary (RVS) are marked. The synthetic spectrum of the secondary is drawn with the proper radial velocity shift. The corresponding lines in the primary and secondary component are outlined using arrows. Dots above the echelle spectrum designate positions of telluric lines contaminating the stellar spectrum, some of them are marked with vertical bars. The spectra are shifted down by 0.2 in ordinate intensity for clarity.